Biochemical Journal (2022) **479** 1317–1336
https://doi.org/10.1042/BCJ20220170

PORTLAND PRESS

Research Article

Inhibition of basal and glucagon-induced hepatic glucose production by 991 and other pharmacological AMPK activators

Manuel Johanns[1], Cyril Corbet[2], Roxane Jacobs[1], Melissa Drappier[1], Guido T. Bommer[1], Gaëtan Herinckx[1], Didier Vertommen[1], Nicolas Tajeddine[3], David Young[4], Joris Messens[4], Olivier Feron[2], Gregory R. Steinberg[5], Louis Hue[1] and Mark H. Rider[1]

[1]Université Catholique de Louvain (UCLouvain) and de Duve Institute (DDUV), Avenue Hippocrate 75, 1200 Brussels, Belgium; [2]Université Catholique de Louvain (UCLouvain) and Institute of Experimental and Clinical Research (IREC), Pole of Pharmacology and Therapeutics (FATH), Avenue Hippocrate 57, 1200 Brussels, Belgium; [3]Université Catholique de Louvain (UCLouvain) and Institute of Neuroscience (IONS), Avenue Hippocrate 53, 1200 Brussels, Belgium; [4]Vrije Universiteit Brussels (VUB) and VIB Center for Structural Biology, Pleinlaan 2, 1050 Brussels, Belgium; [5]Centre for Metabolism, Obesity and Diabetes Research, Department of Medicine and Department of Biochemistry and Biomedical Sciences, McMaster University, Hamilton, Ontario, Canada

Correspondence: Mark H. Rider (mark.rider@uclouvain.be)

Pharmacological AMPK activation represents an attractive approach for the treatment of type 2 diabetes (T2D). AMPK activation increases skeletal muscle glucose uptake, but there is controversy as to whether AMPK activation also inhibits hepatic glucose production (HGP) and pharmacological AMPK activators can have off-target effects that contribute to their anti-diabetic properties. The main aim was to investigate the effects of 991 and other direct AMPK activators on HGP and determine whether the observed effects were AMPK-dependent. In incubated hepatocytes, 991 substantially decreased gluconeogenesis from lactate, pyruvate and glycerol, but not from other substrates. Hepatocytes from AMPKβ1$^{-/-}$ mice had substantially reduced liver AMPK activity, yet the inhibition of glucose production by 991 persisted. Also, the glucose-lowering effect of 991 was still seen in AMPKβ1$^{-/-}$ mice subjected to an intraperitoneal pyruvate tolerance test. The AMPK-independent mechanism by which 991 treatment decreased gluconeogenesis could be explained by inhibition of mitochondrial pyruvate uptake and inhibition of mitochondrial *sn*-glycerol-3-phosphate dehydrogenase-2. However, 991 and new-generation direct small-molecule AMPK activators antagonized glucagon-induced gluconeogenesis in an AMPK-dependent manner. Our studies support the notion that direct pharmacological activation of hepatic AMPK as well as inhibition of pyruvate uptake could be an option for the treatment of T2D-linked hyperglycemia.

Introduction

Type 2 diabetes (T2D) is a metabolic disorder characterized by elevated blood glucose (hyperglycemia), even in the starved state, due to decreased glucose utilization and disposal in peripheral tissues, mainly skeletal muscle [1,2], although insulin resistance, particularly in liver, makes an important contribution to hyperglycemia in T2D patients during starvation. The disease is also characterized by increased hepatic glucose production (HGP) exacerbated by glucagon, whose levels are increased in T2D [3]. Under normal conditions during short-term starvation, glucagon secretion tends to maintain glycemia by increasing glycogen breakdown and by favoring gluconeogenesis (GNG) over glycolysis in liver [4]. The mechanism of action of glucagon involves G-protein-coupled plasma membrane adenylate cyclase activation, thereby increasing adenosine 3′,5′-cyclic monophosphate (cAMP) production [5]. Increased cAMP leads to cAMP-dependent protein kinase (PKA) activation [6]. PKA phosphorylates liver 6-phosphofructo-2-kinase (PFK-2)/fructose-2,6-bisphosphatase (PFKFB1)

Received: 14 April 2022
Revised: 2 June 2022
Accepted: 7 June 2022

Accepted Manuscript online: 7 June 2022
Version of Record published: 22 June 2022

Biochemical Journal (2022) 479 1317–1336
https://doi.org/10.1042/BCJ20220170

to lower fructose-2,6-bisphosphate concentration [7–9], and by phosphorylating and inactivating liver-type pyruvate kinase, glycolysis is inhibited [10,11]. These acute effects of glucagon to decrease fructose-2,6-bisphosphate levels and inactivate pyruvate kinase partly explain how the hormone stimulates HGP. In the long-term, glucagon increases the expression of the key gluconeogenic enzymes, glucose-6-phosphatase (G6Pase) and phosphoenolpyruvate carboxykinase (PEPCK) [12,13]. Together these short- and long-term effects increase net glucose output by the liver to maintain glucose homeostasis during starvation.

AMP-activated protein kinase (AMPK) is a well-recognized drug target for treating T2D [14]. We showed that AMPK activation in hepatocytes leads to cyclic nucleotide phosphodiesterase-4B (PDE4B) activation, antagonizing glucagon-induced cAMP accumulation and downstream PKA signaling [15]. Historically, AMPK activation in skeletal muscle upon contraction was first shown to lead to insulin-independent stimulation of glucose uptake [16], partly explaining the beneficial effects of exercise for managing the disease. Thereafter, metformin was found to activate AMPK in liver [17], but whether AMPK activation is responsible for decreased HGP is controversial. Treatment with 5-aminoimidazole-4-carboxamide riboside (AICAR) or metformin at 'therapeutic' doses (below 100 μM) effectively reduced HGP and led to AMPK activation. However, the use of transgenic mouse models suggested that these effects as well as glucose uptake and phosphorylation were mostly AMPK-independent [18,19]. In contrast, genetic ablation of AMPKα2 in liver caused hyperglycemia due to increased HGP and impaired capacity of leptin and adiponectin to reduce HGP [20]. Also, short-term overexpression of constitutively active AMPKα2 led to mild hypoglycemia due to reduced HGP [21]. Lastly, mice lacking liver kinase B1 (LKB1), the main upstream AMPK-activating kinase, were hyperglycemic and resistant to metformin treatment [22]. It is thus still unclear whether and how AMPK controls HGP.

Compounds interfering with mitochondrial ATP production, such as metformin [23], activate AMPK indirectly via an increase in intracellular AMP : ATP ratio. AICAR, the first pharmacological AMPK activator, is converted in cells to the AMP analog ZMP [24]. More recently, a novel class of direct activators was discovered that bind to a pocket between the AMPK α- and β-subunits, the so-called 'Allosteric Drug and Metabolite' or 'ADaM' binding site [25]. The first such compound was A769662 [26] that specifically activated AMPKβ1-containing heterotrimers [27,28]. Compound 991 is also AMPKβ1-specific, at least in cell-free assays [28], but at high doses, 991 activated both AMPKβ1- and AMPKβ2-containing complexes in skeletal muscle associated with increased glucose uptake [29]. Recently, several 'pan-β' AMPK direct activators, namely SC4 [30], MK8722 [31] and PF793 [32] have been developed and some have successfully been used *in vivo* to reduce hyperglycemia in rodent models of insulin resistance. Another small-molecule called O304 [33] has entered human clinical trials, but its precise mode of action is uncertain. Although none of these novel compounds were reported to significantly reduce HGP, the question was not always thoroughly addressed, as the main focus was on investigating increased glucose uptake in skeletal muscle induced by compound treatment.

AMPK activation represents an attractive approach for the treatment of T2D, yet pharmacological AMPK activators can have additional targets that contribute to their anti-diabetic effects. Understanding these side effects might reveal novel therapeutic treatments. In the present study we investigated whether 991 affects HGP from a variety of substrates in freshly isolated mouse hepatocytes. We also tested effects of intraperitoneal administration of 991 to high-fat diet (HFD)-induced insulin resistant mice and to AMPKβ1$^{-/-}$ mice on a normal chow diet using an intraperitoneal pyruvate tolerance test (IPPTT). New-generation direct small-molecule AMPK activators were found to antagonize glucagon-induced HGP in an AMPK-dependent manner. Our studies unravel both AMPK-independent and AMPK-dependent mechanisms by which 991 inhibits HGP and support the notion that pharmacological hepatic AMPK activation as well as inhibition of pyruvate uptake could be an option for the treatment of T2D-linked hyperglycemia.

Results

AMPK activator 991 inhibits GNG from various substrates

We previously reported that AMPK activation in primary mouse hepatocytes antagonizes glucagon signaling [15]. In line with this study, incubation of freshly isolated hepatocytes from overnight-starved mice (to deplete liver glycogen) with 991 decreased glucose production by more than 75% from the classically used gluconeogenic substrate mixture of lactate plus pyruvate in a physiological 10 : 1 molar ratio (Figure 1A). Remarkably, the inhibition of GNG by 991 was observed not only in the presence of glucagon, but also under basal conditions (Figure 1A). GNG inhibition by 991 was dose-dependent and incubation with 10 μM 991 resulted in ∼85% inhibition of glucose production (Figure 1B). It was recently shown that metformin can inhibit hepatic GNG *in vivo* from

Biochemical Journal (2022) **479** 1317–1336
https://doi.org/10.1042/BCJ20220170

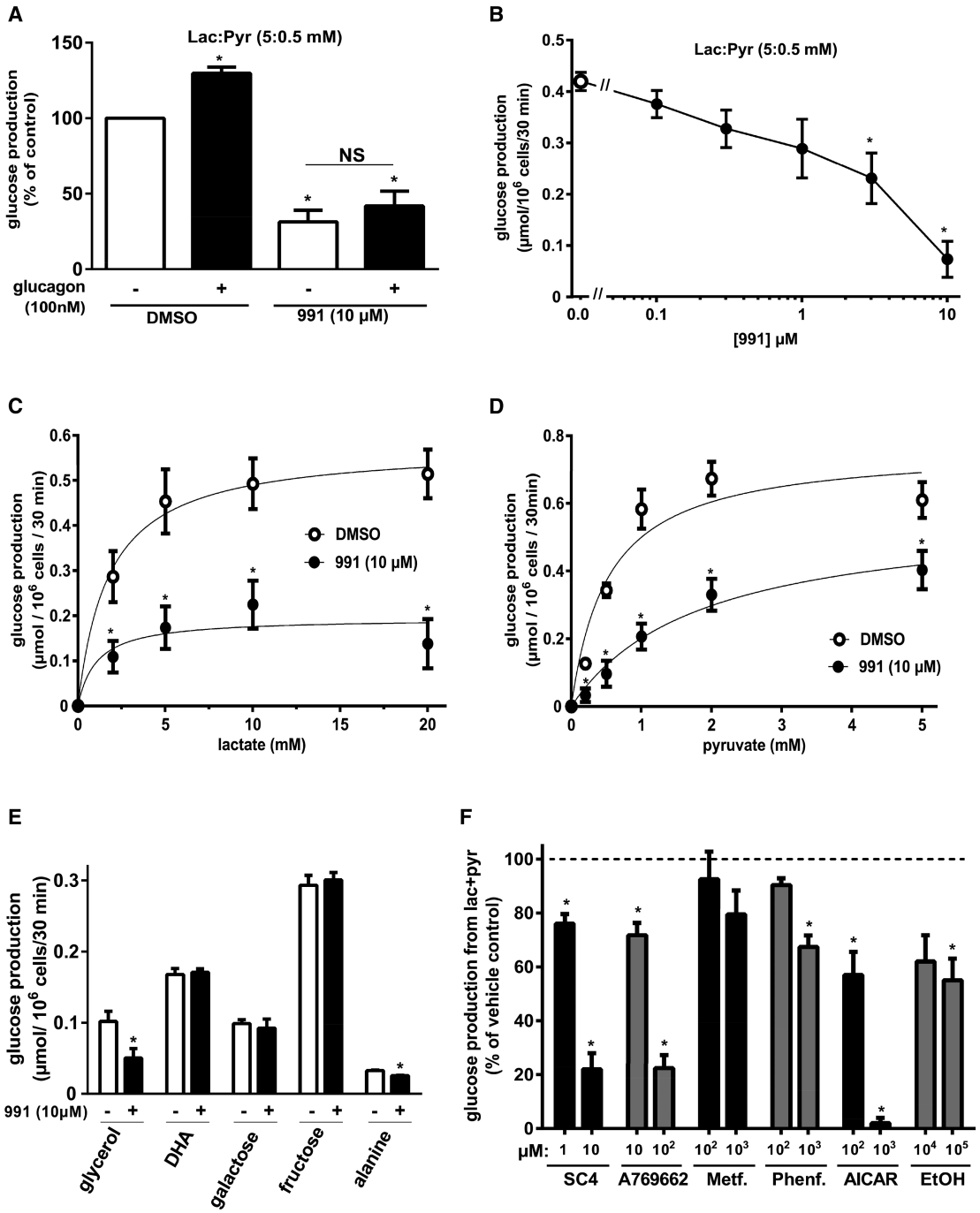

Figure 1. Effects of 991 on HGP from lactate, pyruvate and other substrates.

Freshly isolated mouse hepatocytes were incubated for 30 min with the indicated concentrations of compounds or 0.1% DMSO as vehicle control, for measurements of medium glucose from different substrates: 5 mM lactate (Lac) + 0.5 mM pyruvate (Pyr) (**A**,**B**,**F**); from the indicated concentrations of either lactate (**C**) or pyruvate (**D**) alone; or from 5 mM of either glycerol, dihydroxyacetone (DHA), galactose, fructose or alanine (**E**). Incubation media contained no glucose but contained 0.5 mM sodium octanoate as energy substrate. The hyperbolic curves that are traced in panels (**C**) and (**D**) were obtained by fitting the mean data to the Michaelis–Menten equation. The data are means ± S.E.M. of 7 (**A**), 4 (**B**,**C**,**D**) or 3 (**E**,**F**) separate experiments and * indicates a significant difference ($P < 0.05$) compared with vehicle controls (paired *t*-test).

Biochemical Journal (2022) 479 1317–1336
https://doi.org/10.1042/BCJ20220170

reduced substrates such as lactate, but not from oxidized substrates such as pyruvate [34]. Therefore, we investigated effects of 991 on glucose production from different substrates. From either lactate or pyruvate alone, glucose production increased dose-dependently, reaching a plateau at ∼20 mM lactate (Figure 1C) or at ∼2 mM pyruvate (Figure 1D). A global best-fit of the mean data to the Michaelis–Menten equation gave V_{max} and K_M values of 0.58 µmol/10^6 cells/30 min and 1.8 mM for control incubations and 0.19 µmol/10^6 cells/30 min and 1.1 mM for incubations with 991 from lactate; and V_{max} and K_M values of 0.76 µmol/10^6 cells/30 min and 0.53 mM for control incubations and 0.57 µmol/10^6 cells/30 min and 1.8 mM for incubations with 991 from pyruvate. Incubation with 991 thus decreased glucose production from both substrates at all concentrations tested, but the effect of 991 on GNG from lactate was mainly to decrease maximal glucose production (Figure 1C), whereas its effect on GNG from pyruvate mainly affected substrate concentration-dependence (Figure 1D). This difference might be due to changes in substrate transport and/or in intracellular concentrations of pyruvate resulting from the lactate dehydrogenase (LDH) reaction and in direct link with the cytosolic redox state (see below).

To pinpoint steps where 991 might act, we measured glucose production from alternative substrates. Interestingly, while 991 had no effect on HGP from dihydroxyacetone, galactose or fructose, it slightly decreased GNG from alanine (∼25%), and markedly decreased GNG from glycerol (∼50%) (Figure 1E), suggesting possible inhibition of *sn*-glycerol-3-phosphate (Gro3P) dehydrogenase-1/2 (GPD1/2) by 991 (see below). It is worth mentioning that HGP from glycerol makes an important contribution to total glucose production during prolonged starvation [35] or in obesity [36] when adipose tissue lipolysis is high.

Next, we compared the effect of 991 on GNG with other direct AMPK activators. Incubation with SC4 and A769662 effectively inhibited glucose production at concentrations of 10 µM and 100 µM, respectively, whereas metformin and phenformin treatment, even at concentrations of 1 mM, only had modest effects (Figure 1F). Incubation with 1 mM AICAR almost totally blocked glucose production, probably through AMPK-independent inhibition of fructose-1,6-bisphosphatase (FBPase-1) by ZMP [37].

Direct inhibition of mitochondrial GPD2 by metformin might increase the cytosolic NADH : NAD^+ ratio and was recently proposed to be involved in its blood glucose lowering effect in rats [38]. When hepatocytes were incubated with a high concentration of ethanol (0.1 M), known to rapidly increase the cytosolic NADH : NAD^+ ratio, we observed a modest inhibition of glucose production (Figure 1F). We therefore examined whether the inhibition of GNG by 991 might be due to GPD2 inhibition. Although metformin and 991 have very different chemical structures, we tested whether 991 might directly inhibit GPD2. The activity of purified recombinant mouse GPD2 was inhibited dose-dependently by 991 with an IC_{50} value of ∼25 nM (Figure 2A). When assayed in the presence of increasing concentrations of 991, the V_{max} of GPD2 decreased accompanied by an increase in K_M for Gro3P (Figure 2B,C) suggesting noncompetitive mixed inhibition. GPD2 contains very tightly, but not covalently, bound FAD that even remains in the enzyme after multi-step purification from tissues [39]. We did try to measure GPD2-bound FAD by fluorescence but no changes indicative of displacement were apparent upon addition of 991. Also, GPD2 inhibition by 991 was not competed out by inclusion of additional FAD in the assay (data not shown). It is therefore possible that 991 might interfere with electron transfer to and from bound FAD (see below). Interestingly, incubation of GPD2 with SC4 inhibited GPD2 with similar potency to that seen with 991 (Supplementary Figure S2A, IC_{50} value = ∼20 nM), but no inhibition was seen in the presence of A769662 up to a concentration of 100 µM (Supplementary Figure S2B). We were also able to confirm GPD2 inhibition by metformin (Supplementary Figure S2C), although the IC_{50} value of ∼20 µM was lower than the values of 50–100 µM previously reported [38], but was about three orders of magnitude greater than that observed for the inhibition of GPD2 by 991 and SC4.

In intact rat liver mitochondria, the effect of 991 or metformin on oxygen consumption rate (OCR) was measured from different substrates with respiratory chain inhibitors (Figure 2D). In the presence of pyruvate and malate to generate NADH, phenformin and to a lesser extent metformin inhibited complex I of the respiratory chain as expected, whereas 991 was without effect. None of the compounds affected OCR from succinate via complex II or from TMPD/ascorbate via complex IV (Supplementary Figure S3). From Gro3P as substrate on the other hand, 991 inhibited respiration via complex II by ∼80%, while phenformin and metformin had less pronounced effects (∼50% inhibition, Figure 2D,E). When mitochondrial GPD2 was assayed *in situ* by measuring cytochrome c reduction from Gro3P, incubation with 991 inhibited GPD2 activity by ∼60% at 10 µM (Figure 2F).

Virtual docking experiments using bacterial Gro3P oxidase as template [38] suggested that 991, similar to metformin and phenformin, most likely binds to the FAD-containing pocket of GPD2 (Figure 2G). In lieu of a crystal structure of 991 bound to GPD2, an *in silico* docking approach was used to probe potential binding sites using a homology model of GPD2. Simulations in Autodock Vina yielded a clear preference for the FAD

Biochemical Journal (2022) **479** 1317–1336
https://doi.org/10.1042/BCJ20220170

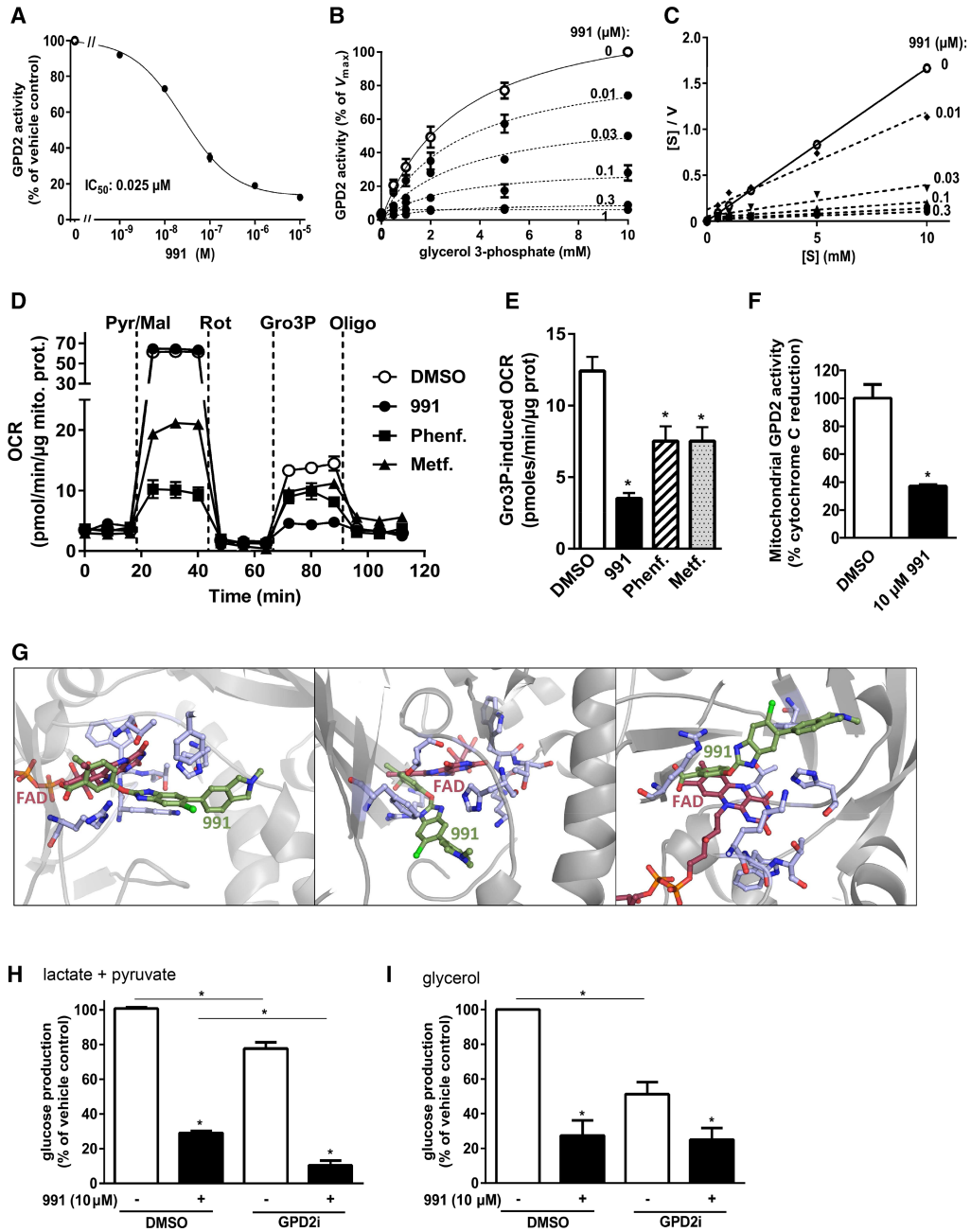

Figure 2. Effects of 991 on GPD2 activity, OCR together with *in silico* molecular docking. Part 1 of 2

(**A**–**C**) Bacterially expressed purified recombinant mouse GST-GPD2 was assayed for DCPIP reduction from Gro3P as substrate in the presence of the indicated concentrations of 991 or DMSO as vehicle control. The effect of increasing concentrations of 991 on the Gro3P saturation curves of GPD2 (**B**) was assessed for the determination of kinetic parameters using a Hanes-Woolf plot (**C**). In (**D**) and (**E**), OCRs of freshly isolated rat liver mitochondria were measured by Seahorse^{TM} in the presence of 10 mM pyruvate (Pyr), 2.5 mM malate (Mal), 1 µM rotenone (Rot), 10 mM Gro3P, 1 µM oligomycin (Oligo) after pre-incubation for 1 h with 10 µM 991, 100 µM phenformin, 100 µM metformin or DMSO as vehicle control. In (**F**) GPD2 activity in freshly isolated intact mitochondria was measured as reduction of added cytochrome c from Gro3P as substrate after pre-incubation with 991 or DMSO as vehicle control. In (**G**) compound 991 was docked to a homology model of GPD2 by *in silico* simulation. The favored docking conformation places 991 (green) in close proximity to the flavin of the bound FAD (red) and several key active site residues (blue) previously highlighted in α-glycerophosphate oxidase [40]. The residues shown are GPD2 residues equivalent to α-glycerophosphate oxidase Thr61, Leu63, His65, Phe286, Arg346, Lys429, Ile430 (tryptophan in GPD2), and Thr431. Glucose production from lactate + pyruvate (**H**) or from glycerol (**I**) was measured as in Figure 1 with

Biochemical Journal (2022) **479** 1317–1336
https://doi.org/10.1042/BCJ20220170

Figure 2. Effects of 991 on GPD2 activity, OCR together with *in silico* molecular docking. Part 2 of 2
100 μM GPD2 inhibitor (GPD2i) STK017597 and/or 10 μM 991 or DMSO as vehicle control. The data are means ± S.E.M. of 5 (**A**) or 3 (**B**,**C**,**E**,**F**,**H**,**I**) separate experiments and * indicates a significant difference ($P < 0.05$) compared with vehicle controls (paired *t*-test). The data in (**D**) are from one representative experiment with six technical replicates.

binding site of GPD2 as the docking location for 991. The majority of the binding conformations of 991 clustered at the active site of GPD2, with the most favorably bound conformation (based on an estimated binding affinity of 991 at this position of −11 kcal/mol) effectively blocking the region between the flavin part of FAD and key residues of the active site inferred from the homologous α-glycerophosphate oxidase [40].

Interestingly, incubation of hepatocytes with the known GPD2 inhibitor STK017597 only led to a modest (∼20%) decrease in glucose production from lactate : pyruvate (Figure 2H), suggesting that GPD2 inhibition alone cannot fully account for the inhibition of glucose production from these substrates by 991. On the other hand, GPD2 inhibition by 991 could explain the inhibition of glucose production from glycerol (Figure 1E) and indeed both 991 and STK017597 inhibited glucose production from glycerol (Figure 2I). The fact that there was no synergistic effect of 991 and the GPD2 inhibitor on glucose production from glycerol compared with 991 alone suggests the same underlying mechanism of inhibition of GNG, namely inhibition of GPD2. Of note, *in vitro* phosphorylation studies identified Ser462 as a major AMPK phosphorylation site in mouse GPD2 (Supplementary Figure S1). However, we were unable to detect any effect of *in vitro* phosphorylation of recombinant GST-GPD2 by AMPK on GPD2 activity (data not shown). Interestingly, yeast GPD2 was phosphorylated and inactivated by the yeast AMPK homolog SNF1, proposed to limit glycerol production when nutrients are scarce [41]. However, the equivalent site (Ser266) was not identified as a phosphorylation site for AMPK in mouse GPD2.

Effect of 991 on cytosolic redox state

Metformin has been proposed to affect the intracellular redox balance, favoring a more reduced state (a higher NADH : NAD^+ ratio), thereby limiting GNG from reduced substrates such as lactate that need to be oxidized in a reaction producing NADH [34,38]. We compared effects of increasing concentrations of 991, SC4, A769662, metformin and phenformin, including doses inducing maximal AMPK activation in hepatocytes, on the activity of purified dehydrogenases that constitute major redox shuttles between the cytosol and the mitochondrial matrix, namely cytosolic GPD1/mitochondrial GPD2 of the glycerol phosphate shuttle, cytosolic malate dehydrogenase-1 (MDH1)/mitochondrial malate dehydrogenase-2 (MDH2) of the malate-aspartate shuttle along with LDH. Incubation with 10 μM 991 had no effect on GPD1 or LDH activity, had no effect on MDH2 activity, partly inhibited MDH1 activity (∼60%), but inhibited GPD2 activity by ∼90% (Supplementary Figure S2D). SC4 (10 μM) also inhibited MDH1 (∼90%) and MDH2 (∼60%) and, like compound 991, strongly inhibited GPD2 with little or no effect on LDH and GPD1 activity, respectively. Metformin and phenformin, on the other hand, had no effect on GPD1, MDH1/2 or LDH activities, but strongly inhibited GPD2 activity even at the lower dose of 100 μM (Supplementary Figure S2D). A769662 did not significantly inhibit GPD2, but strongly inhibited (>80%) the other dehydrogenases at the highest dose of 100 μM. Of note, incubation with up to 10 μM 991 had no effect on the activities of purified glyceraldehyde phosphate dehydrogenase (GAPDH), purified glutamate dehydrogenase or succinate dehydrogenase/complex II activity in mitochondrial preparations (Supplementary Figure S2E–G).

Conventional methods to assess the cytosolic NADH : NAD^+ ratio often rely on calculations based on substrate : product concentration ratios, such as measurements of the lactate : pyruvate ratio from the equilibrium LDH reaction. Otherwise, total nicotinamide dinucleotide concentrations can be measured in deproteinized extracts, yet most intracellular NADH/NAD^+ is probably protein-bound and only the free forms are relevant for the control of redox reactions. Therefore, we took advantage of the recently developed 'Peredox' probe [42], introduced by lentiviral expression in immortalized human hepatocyte (IHH) cells [43], to monitor real time changes in free cytosolic NADH by fluorescence of the probe due to NADH binding. Live-cell imaging for up to 30 min revealed that 991 did not alter the basal redox state in the presence of glucose alone (Supplementary Figure S5A), consistent with the fact that under normal conditions the Gro3P shuttle makes only a minor contribution to the total flux of reducing equivalents from the cytosol to mitochondria. The addition of lactate

rapidly increased fluorescence reaching a maximum after ∼5 min, after which the addition of pyruvate led to a time-dependent decrease in fluorescence that plateaued off at a minimum level below basal at 20 min (Supplementary Figure S5A). The addition of pyruvate led to a time-dependent decrease in basal fluorescence that was unaffected by the addition of lactate thereafter (Supplementary Figure S5A) Interestingly, the increase in fluorescence induced by lactate was decreased by 991 in a manner similar to that of pyruvate, indicating that 991 might alter the lactate : pyruvate ratio (Supplementary Figure S5A). Strikingly, incubation with 991 prior to addition of lactate completely prevented lactate-induced increases in fluorescence (Supplementary Figure S5A) suggesting a possible interference with cellular lactate uptake and/or subsequent pyruvate transport across mitochondria.

It is noteworthy that incubation with 991 did not prevent or reverse the increase in fluorescence induced by other reduced substrates, xylitol or ethanol (Supplementary Figure S5C), suggesting that the effect was specific for lactate. Neither metformin nor phenformin, at doses up to 1 mM, altered changes in NADH fluorescence in response to the addition of different substrates including lactate in these short-term incubations, whether added before or after the substrate (Supplementary Figure S5B). Therefore, IHH cells expressing the Peredox probe were incubated up to 24 h for IncuCyte® live cell imaging. In the presence of lactate and pyruvate (10 : 1 ratio), the fluorescence signal of the NADH probe slowly decreased over time, and this was exacerbated in the presence of 991, but partly prevented by the addition of phenformin, whereas metformin only slightly increased fluorescence compared with control incubations (Supplementary Figure S6).

Effect of 991 on intermediary metabolite levels

To further investigate effects of 991 on glucose production, metabolite concentrations relevant to GNG were measured by GC–MS in freshly isolated mouse hepatocytes incubated without (glucose only) or with gluconeogenic substrates lactate, pyruvate or both together in a 10 : 1 ratio (Figure 3 and Supplementary Figure S4). The only metabolite whose relative concentration consistently increased in response to 991 treatment, regardless of the gluconeogenic substrates, was Gro3P (Figure 3A), coherent with GPD2 inhibition. Relative levels of several other metabolites such as glucose 6-phosphate (G6P) decreased upon 991 treatment (Figure 3B). The most marked decreases were seen for 3-phosphoglycerate (3PG) and phosphoenolpyruvate (PEP) levels (Figure 3C,D), suggesting that the gluconeogenic step inhibited by 991 was upstream of PEPCK, thus potentially a mitochondrial step. Interestingly, in the presence of pyruvate (alone or in combination with lactate), a decrease in aspartate levels was also seen upon treatment with 991 (Figure 3E), suggesting that either pyruvate carboxylase activity or pyruvate transport was affected by 991 treatment. Surprisingly, there were no significant differences in citrate, pyruvate or lactate levels in hepatocytes incubated with 991 irrespective of the gluconeogenic substrates (Figure 3F–H), suggesting that these metabolites are rapidly converted to products of near-equilibrium reactions or that differences are compartmentalized and thus cannot be seen in full-cell extracts.

Compound 991 inhibits mitochondrial pyruvate transport

As pyruvate carboxylase and pyruvate dehydrogenase are both located in the mitochondrial matrix, pyruvate has to be actively transported across the mitochondrial membrane to be further metabolized. The mitochondrial pyruvate carrier (MPC) uses the mitochondrial proton gradient to transport pyruvate from the cytosol to the mitochondrial matrix. In freshly isolated mouse hepatocytes, 991 treatment decreased glucose production from lactate : pyruvate by ∼70% while incubation with UK5099, an inhibitor of the MPC, almost completely abrogated glucose production (Figure 4A). Hepatocyte glucose production from pyruvate alone was also inhibited to a similar extent by 991 but when glucose production was measured from methyl pyruvate, which freely crosses cell membranes thus circumventing the MPC, the effect of 991 to decrease HGP was abolished (Figure 4B). To evaluate the implication of AMPK activation in the inhibition of GNG by 991, we resorted to the use of hepatocytes from wild-type (WT) mice and from mice bearing a whole-body deletion of AMPKβ1 (AMPKβ1$^{-/-}$). In cell-free assays, 991 more potently activates AMPKβ1-containing than AMPKβ2-containing complexes [28] and rodent liver predominantly expresses AMPKα2β1γ1 [44]. Indeed, total AMPK activity was reduced by ∼80% in extracts from AMPKβ1$^{-/-}$ versus WT hepatocytes incubated with or without compound 991 (Figure 4C) and effects of 991 treatment to increase AMPKα Thr172 as well as downstream acetyl-CoA carboxylase (ACC) and regulatory-associated protein of mammalian target of rapamycin (Raptor) phosphorylation were almost completely abrogated in AMPKβ1$^{-/-}$ versus WT hepatocytes (Figure 4D).

Using an inhibitor-stop technique to measure radioactive pyruvate uptake by intact rat liver mitochondria [45], we found that pyruvate transport was reduced by ∼60% after pre-incubation with 991, while ∼40% inhibition was

Biochemical Journal (2022) **479** 1317–1336
https://doi.org/10.1042/BCJ20220170

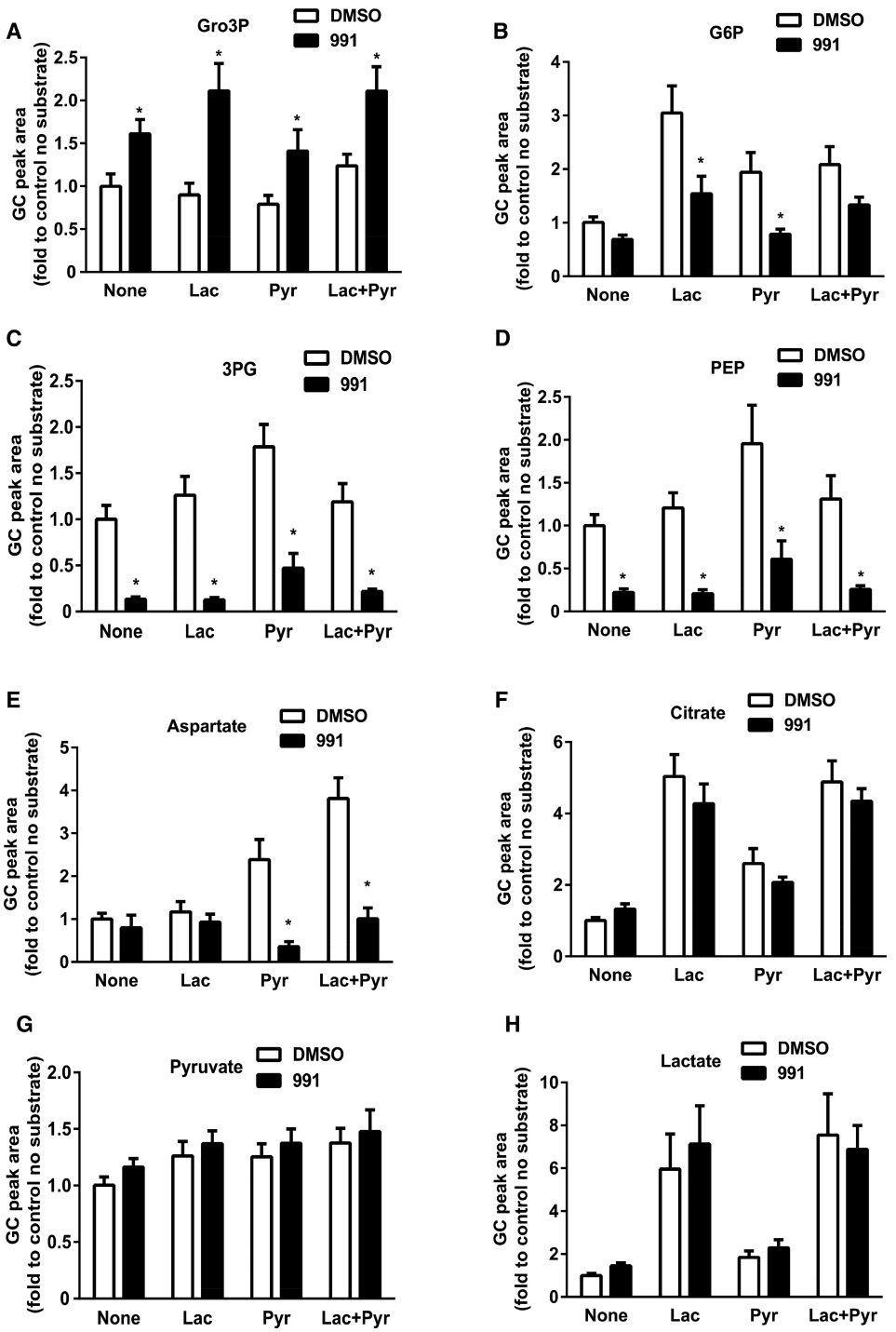

Figure 3. Effects of 991 on metabolite levels by GC–MS in hepatocytes incubated with lactate, pyruvate or lactate + pyruvate.

Freshly isolated mouse hepatocytes were incubated for 30 min in medium containing 5.5 mM glucose (None), 5 mM lactate (Lac), 1 mM pyruvate (Pyr) or 5 mM lactate + 0.5 mM pyruvate (Lac + Pyr) along with 10 μM 991 or DMSO as vehicle control for measurements of relative metabolite levels of Gro3P (**A**), G6P (**B**), 3PG (**C**), PEP (**D**), aspartate (**E**), citrate (**F**), pyruvate (**G**) and lactate (**H**) by GC–MS. The data are means ± S.E.M. of six separate experiments and * indicates a significant difference ($P < 0.05$) compared with vehicle controls (two-way ANOVA with an appropriate *post-hoc* test).

Biochemical Journal (2022) **479** 1317–1336
https://doi.org/10.1042/BCJ20220170

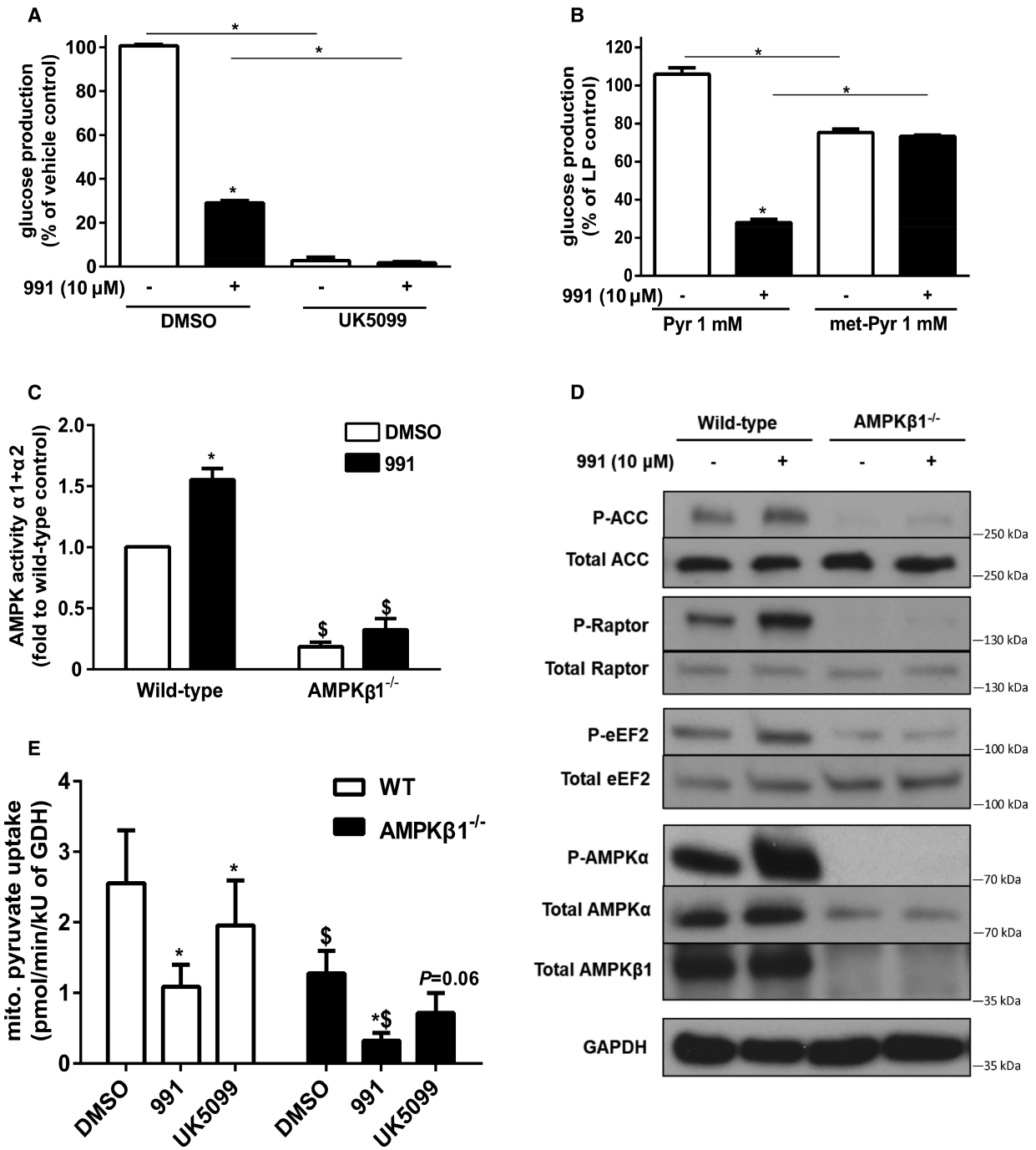

Figure 4. Effects of 991 on AMPK activity and mitochondrial pyruvate uptake in WT versus AMPKβ1$^{-/-}$ mice.

In (**A**) and (**B**), glucose production from 5 mM lactate + 0.5 mM pyruvate (**A**), 1 mM pyruvate (Pyr) or 1 mM methyl-pyruvate (met-Pyr) (**B**) was measured in freshly isolated mouse hepatocytes incubated as described in the legend to Figure 1 with 10 μM 991 or 10 μM UK5099 or with DMSO (vehicle control; values are expressed as percent of vehicle control with lactate + pyruvate). Freshly isolated hepatocytes from WT or AMPKβ1$^{-/-}$ mice were incubated for 30 min in medium containing 10 mM glucose and 10 μM 991 or DMSO as vehicle control for measurement of total AMPK activity in lysates following immunoprecipitation with anti-AMPKα1 + anti-AMPKα2 antibodies (**C**) or for immunoblotting with the indicated antibodies (**D**). Pyruvate uptake by mitochondria freshly isolated from WT or AMPKβ1$^{-/-}$ mouse livers (**E**) was measured using a rapid inhibitor-stop technique with [^{14}C]-pyruvic acid after pre-incubation with DMSO (vehicle control), 10 μM 991 or 10 μM of the MPC inhibitor UK5099. The data are means ± S.E.M. of 3 (**A**,**B**,**C**) or 5 (**E**) separate experiments and * indicates a significant difference ($P < 0.05$) compared with vehicle controls (paired *t*-test; **A**,**B**,**C** or by two-way ANOVA followed by an appropriate *post-hoc* test; **E**).

Biochemical Journal (2022) 479 1317–1336
https://doi.org/10.1042/BCJ20220170

seen in mitochondria pre-incubated with MPC inhibitor UK5099 (Figure 4E). The effects of 991 and UK5099 treatment to decrease mitochondrial pyruvate uptake were similar in hepatocytes from WT and from AMPKβ1$^{-/-}$ mice, although absolute values of pyruvate uptake were reduced by ∼50% in hepatocytes from the knockout mice (Figure 4E). These results suggest that the inhibition of mitochondrial pyruvate uptake by 991 does not involve AMPK.

Role of AMPK in the inhibition of GNG by 991 in incubated hepatocytes and on HGP *in vivo*

Although effects of 991 on AMPK activation and target phosphorylation were AMPKβ1-dependent (Figure 4C,D), the 991-induced reduction in basal glucose production from either lactate or pyruvate alone or in combination was similar in hepatocytes from WT versus AMPKβ1$^{-/-}$ mice (Figure 5A), indicating that AMPK activity does not affect basal GNG. We next looked whether 991 could lower glycemia in diabetic mice *in vivo*. Compound 991 was administered intraperitoneally to overnight starved high-fat diet (HFD)-induced insulin resistant mice and plasma

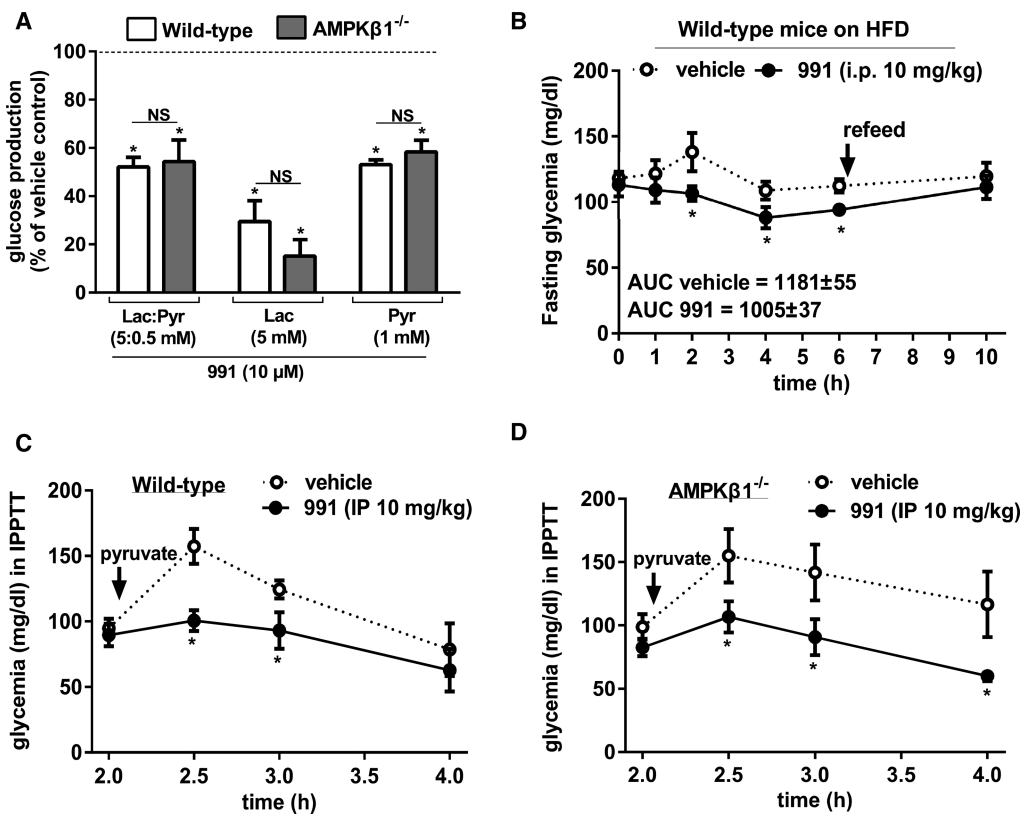

Figure 5. Effects of 991 on glucose production in hepatocytes from WT versus AMPKβ1$^{-/-}$ mice together with *in vivo* measurements of fasting glycemia in insulin-resistant mice and IPPTT in WT versus AMPKβ1$^{-/-}$ mice.

Freshly isolated hepatocytes from WT or AMPKβ1$^{-/-}$ mice were incubated for 30 min in medium without glucose but with the indicated substrates for measurement of glucose production (**A**). Basal levels of glucose production (DMSO condition), expressed as fold of AMPKβ1$^{-/-}$ versus WT, were for Lac + Pyr: 1.3 ± 0.4; Lac: 1.2 ± 0.4; Pyr: 0.9 ± 0.1. In (**B**) HFD-induced diabetic mice were starved overnight and fasting glycemia was measured at the indicated intervals after intraperitoneal (i.p.) injection of 991 (dose of 10 mg per kg body weight) or DMSO as vehicle control. Standard diet-fed WT (**C**) and AMPKβ1$^{-/-}$ (**D**) mice without access to food were subjected to an intraperitoneal pyruvate tolerance test (IPPTT, 1 g sodium pyruvate per kg body weight) 2 h after injection of 991 or DMSO. In (**A**) the data are means ± S.E.M. of three separate experiments and * indicates a significant difference ($P < 0.05$) compared with vehicle controls (paired *t*-test). The data in (**B**) and (**C**,**D**) are from experiments with 5–7 animals per group and * indicates a significant difference ($P < 0.05$) compared with vehicle controls (unpaired *t*-test).

Biochemical Journal (2022) 479 1317–1336
https://doi.org/10.1042/BCJ20220170

glucose concentrations were measured over time. Compound 991 only slightly decreased glycemia from 2–6 h after administration (Figure 5B) and the effect was lost following refeeding. To test whether the glucose lowering effect of 991 was due to a reduction in HGP and whether this implicated AMPK, WT versus AMPKβ1$^{-/-}$ mice maintained on a standard chow diet were starved overnight and injected with 991 for an IPPTT. In WT and AMPKβ1$^{-/-}$ mice, basal glycemia was unaffected by administration of 991, suggesting that skeletal muscle glucose uptake would not have been affected by 991. Indeed, skeletal muscle predominantly expresses AMPKα2β2-containing trimers that are much less potently activated by 991 *in vitro* [28,29]. However following pretreatment with 991, the pyruvate-induced increase in glycemia was abrogated both in WT mice and in AMPKβ1$^{-/-}$ mice to about the same extent (Figure 5C,D). The dose of 991 (10 mg/kg) we used was the same as the concentration of pan-AMPK activator MK8722 that was administered *in vivo* with blood glucose lowering effects [31]. From the molecular mass of 991 (432 g/mol) and assuming a dilution space of 50%, this would give a concentration of ∼50 μM. Although 991 binds to serum albumin which lowers its free concentration considerably, the molecule was clearly effective in decreasing blood glucose in the IPPTTs (Figure 5C,D). Taken together, the results suggest that the effect of 991 was mainly on HGP and AMPK-independent.

Effects of small-molecule AMPK activators on basal and glucagon-stimulated GNG

Lastly, we explored effects of 991 together with some recently described pan-AMPK activators and AICAR as a positive control on both basal and glucagon-stimulated glucose production in incubated mouse hepatocytes. Compared with 991 and AICAR treatment, which substantially decreased glucose production from lactate : pyruvate, incubation of mouse hepatocytes with identical concentrations of PF739 or MK8722 only slightly decreased glucose production and O304 was without significant effect (Figure 6A). However, incubation of hepatocytes with each of the compounds increased AMPK Thr172 and ACC Ser79 phosphorylation (Figure 6B). Importantly, glucagon-stimulated increases in glucose production were antagonized in hepatocytes treated with AMPK activators 991, PF739, MK8722 and AICAR (but not O304). Moreover, PF739 and MK8722 treatment significantly counteracted the glucagon effect to increase glucose production in hepatocytes from WT but not in AMPKβ1$^{-/-}$ mice (Figure 6C). We previously showed that the 991-induced reduction in glucagon-stimulated intracellular cAMP levels was abrogated in hepatocytes from AMPKβ1$^{-/-}$ mice [15]. In line with this observation, we show here that glucagon-stimulated PKA activation was significantly reduced by treating hepatocytes with AMPK activators 991, PF7389 and MK8722, and the effect was markedly reduced in hepatocytes from AMPKβ1$^{-/-}$ mice (Figure 6D). The effect of AICAR to decrease PKA activation even in hepatocytes from AMPKβ1$^{-/-}$ mice (Figure 6D) might have been due to the inhibition of adenylate cyclase.

Discussion

AMPK is well recognized as a target for T2D and pharmacological AMPK activation could be a viable strategy to counteract its symptoms. Although there is good evidence that AMPK activation can increase glucose uptake in skeletal muscle, there is controversy in the literature as to whether AMPK activation affects glucose production by the liver. It has been proposed that in response to metformin treatment, decreased GNG could be independent of AMPK [18] and/or indirect due to increased AMP and inhibition of FBPase-1 [37]. We previously showed that AMPK activation by 991 increased glucose uptake in skeletal muscle [29] and antagonized glucagon-induced cAMP/PKA signaling via PDE4B activation in hepatocytes [15]. In the present study we show that, while on the one hand incubation of hepatocytes with 991 reduced basal glucose production mainly via AMPK-independent mechanisms, on the other hand treatment with 991 and other direct pan-AMPK activators antagonized glucagon-stimulated glucose production and cAMP-mediated PKA activation in an AMPK-dependent manner. A scheme summarizing the AMPK-dependent and AMPK-independent mechanisms by which 991 inhibits GNG is shown in Figure 7. AMPK-independent 'off-target' effects of 991 we demonstrated are inhibition of GPD2 and the MPC. Whether 991 directly binds to and inhibits the MPC remains to be established. Direct inhibition of GPD2 by 991 (Figure 2A–C) would account for the observed decrease in glucose production from glycerol in hepatocytes by 991 (Figure 1E) and the rise in intracellular Gro3P (Figure 3A). With lactate : pyruvate as substrate, incubation of hepatocytes with the GPD2 inhibitor STK017597 only modestly decreased glucose production (Figure 2H), suggesting that GPD2 inhibition by 991 cannot fully account for its effect on glucose production. However, with glycerol as substrate, glucose production was strongly (and non-synergistically) inhibited both by 991 and a GPD2 inhibitor (Figure 2I). In

Biochemical Journal (2022) **479** 1317–1336
https://doi.org/10.1042/BCJ20220170

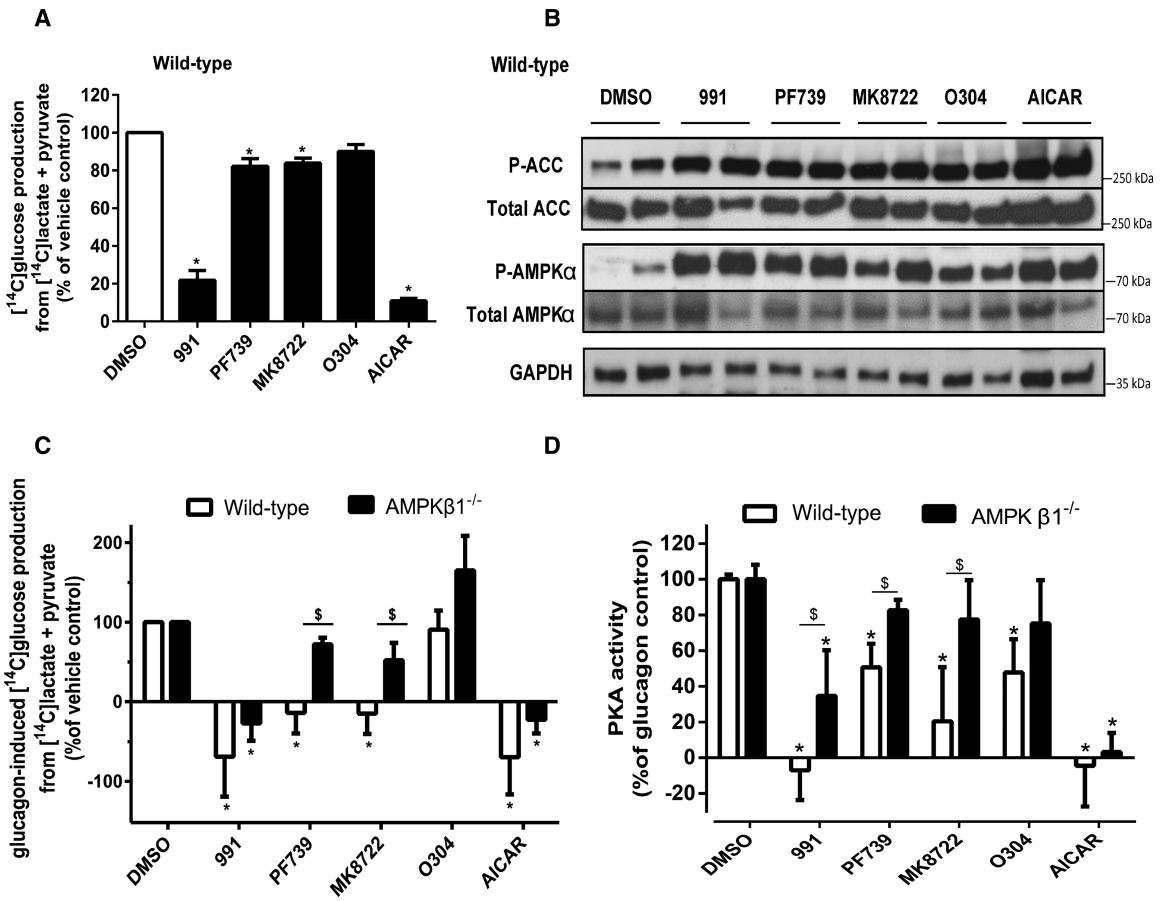

Figure 6. Effects of AMPK activators on basal and glucagon-stimulated glucose production and PKA activity in hepatocytes from WT versus AMPKβ1$^{-/-}$ mice.

Freshly isolated hepatocytes from WT mice were incubated for 30 min with 991 or novel small-molecule AMPK activators (10 μM), 1 mM AICAR or DMSO as vehicle control in medium containing 10 mM glucose for measurement of [^{14}C]-glucose production from lactate + [^{14}C] pyruvate (**A**) or for immunoblotting lysates with the indicated antibodies (**B**). Hepatocytes from WT or AMPKβ1$^{-/-}$ mice were pre-incubated for 30 min with AMPK activators as in (**A**) prior to incubation for 30 min in the presence or absence of glucagon (10 nM) for measurement of [^{14}C]-glucose production from lactate + [^{14}C] pyruvate (**C**) or measurement of PKA activity (**D**). The data are means ± S.E.M. of 6 (**A**) or 4 (**C**,**D**) separate experiments and * indicates a significant difference ($P < 0.05$) compared with vehicle controls (paired *t*-test).

hepatocytes incubated with lactate and pyruvate alone or in combination, there was a marked decrease in intracellular PEP concentration by 991 (Figure 3D), suggesting inhibition at a step preceding PEPCK in the gluconeogenic pathway from lactate or pyruvate. Indeed, 991 inhibited mitochondrial pyruvate uptake (Figure 4E), but did not affect glucose production in hepatocytes incubated with methyl pyruvate, which freely enters mitochondria (Figure 4B). When administered intraperitoneally to HFD-induced insulin-resistant mice, 991 slightly lowered plasma glucose concentrations (Figure 5B) but in chow-fed mice subjected to an IPPTT, the effect of administration of 991 to oppose the rise in glycemia was similar in WT and AMPKβ1$^{-/-}$ mice (Figure 5C,D). Ideally, the IPPTT should be conducted on insulin-resistant mice on a HFD for testing effects of small-molecule AMPK activators (see below), however the AMPKβ1$^{-/-}$ mice would be expected to be more susceptible to develop liver steatosis due to lack of ACC inhibition, thus complicating interpretation of the data.

Lastly, treatment of hepatocytes with recently described potent pan-AMPK activators MK8722 and PF739 barely affected basal glucose production but significantly antagonized glucagon-induced PKA activation (Figure 6D) and glucagon-stimulated glucose production (Figure 6C) in an AMPK-dependent manner. We do believe this short-term anti-glucagon effect of AMPK activation is (patho)physiologically relevant since

Biochemical Journal (2022) **479** 1317–1336
https://doi.org/10.1042/BCJ20220170

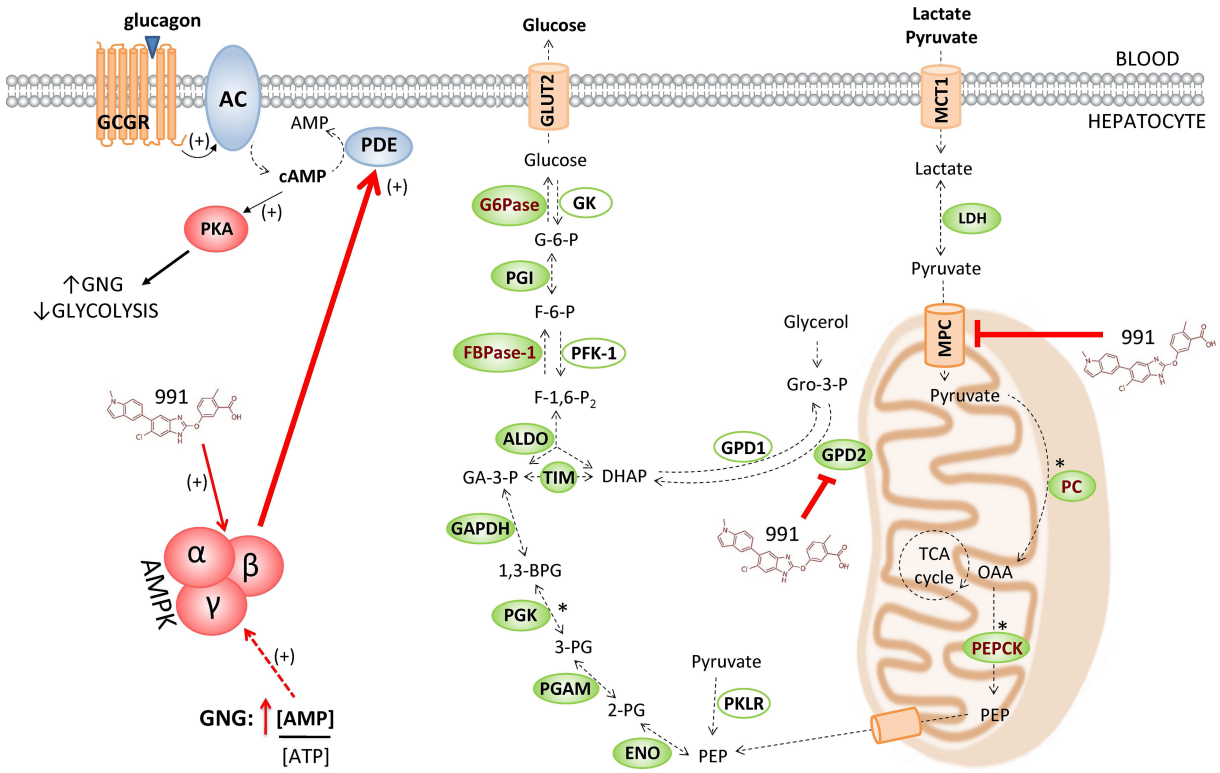

Figure 7. Scheme summarizing the effects of compound 991 and AMPK activation on HGP.

In hepatocytes, an increase in [AMP]:[ATP] ratio resulting from ATP consumption during GNG as wells as 991 and other pharmacological compounds that directly activate AMPK would lead to activation of PDE4B to subsequently decrease cAMP levels, reduce PKA activation and decrease PKA-induced inactivation of liver-type pyruvate kinase (PKLR) and PKA-induced PFK-2 inactivation of PFKFB1 (to raise fructose-2,6-bisphosphate concentration; not shown in the scheme). The net result would be a lowering of glucose production induced by glucagon. In addition, 991 directly inhibits both mitochondrial GPD2 activity and pyruvate transport through the MPC in an AMPK-independent manner, to decrease glucose production from lactate:pyruvate and glycerol. Enzymes involved in GNG are shown in green and those catalyzing key regulatory steps are highlighted in brown. * Indicates energy-consuming (ATP or GTP using) reactions. GCGR, G-protein-coupled glucagon receptor; AC, adenylate cyclase; GLUT2, glucose transporter-2; MCT1, monocarboxylate transporter-1; GK, glucokinase; G-6-P, glucose 6-phosphate; PGI, phosphoglucose isomerase; F-6-P, fructose 6-phosphate; PFK-1, 6-phosphofructo-1-kinase; F-1,6-P_2, fructose 1,6-bisphosphate; ALDO, aldolase; GA-3-P, glyceraldehyde 3-phosphate; TIM, triosephosphate isomerase; DHAP, dihydroxyacetone phosphate; 1,3-BPG, 1,3-bisphosphoglycerate; PGK, phosphoglycerate kinase; 3-PG, 3-phosphoglycerate; PGAM, phosphoglycerate mutase; 2-PG, 2-phosphoglycerate; ENO, enolase; OAA oxaloacetate; PC, pyruvate carboxylase. For other abbreviations, see text.

glucagon levels are abnormally elevated in T2D, which exacerbates HGP. Also, the insulin-sensitizing effects of liver AMPK activation in HFD-induced diabetes by preventing steatosis and insulin-resistance would be beneficial. The experimental presence of glucagon is probably the key to see effects of AMPK activation and, although absent from most *in vitro* hepatocyte incubations, the hormone would be present in starved animals and during the development of diet-induced insulin resistance. Chronic oral administration of a small-molecule AMPK activator ('C24') reduced blood glucose and lipid levels in plasma, reduced hepatic expression of PEPCK and G6Pase and improved the glucose tolerance in diabetic db/db mice [46]. However, based on the administration of direct AMPK activators MK8722, PF249 and PF739 *in vivo*, it was concluded that AMPK activation in the liver would not be significant for glycemic control and that the only beneficial effect of AMPK activation would be in skeletal muscle to increase glucose uptake [31,32]. However, anti-glucagon effects were not studied and even in starved mice timing would be crucial for drug administration since glucagon levels rise and fall transiently. Therefore, we do maintain there is still a case for AMPK activation in the liver to oppose the effects of elevated circulating glucagon levels and improve (hepatic) insulin resistance that characterize

Biochemical Journal (2022) 479 1317–1336
https://doi.org/10.1042/BCJ20220170

T2D. Ideally, drugs should be pan AMPK activators targeted to liver and muscle and avoiding AMPK activation in hypothalamus and heart, which could have adverse effects on food intake and hypertrophy, respectively. Also, AMPK activation should not be too strong or of too long duration to avoid risks of shutting down protein synthesis and causing cell cycle arrest. Further research is thus needed to develop more organ-specific AMPK activators targeting only skeletal muscle and/or liver to minimize unwanted side effects.

Materials and methods

Materials

Compound 991 was kindly provided by Kei Sakamoto (Nestlé, CH) or from CliniSciences (Paris, FR; ref AOB8150-10). SC4 was kindly donated by Jonathan Oakhill (St. Vincent's Institute, University of Melbourne, AU). PF739 and MK8722 were purchased from Glixx Laboratories (Hopkinton, MA, U.S.A.). O304 (synthesized as HY112233 by MedChem Express) was from Bio-Connect (Te Huissen, NL). GPD2 inhibitor STK017597 was from Vitas M Chemical Limited (Hong Kong). Glucagon (reconstituted GlucaGen^{TM}) was from Novo Nordisk. Metformin, phenformin, AICAR and other reagents were from Sigma–Aldrich. Cell culture reagents were from Life Technologies. [γ-^{32}P] ATP, L-[U-^{14}C] lactic acid and [1-^{14}C] pyruvic acid were from PerkinElmer. Anti-total ACC (Merck Millipore, Catalogue No. 04-322), anti-P-Ser79-ACC (Merck-Millipore, Catalogue No. 07-303), anti-GAPDH (Merck-Millipore, Catalogue No. MAB374), anti-total AMPKβ1 (R&D Systems, Catalogue No. AF2854), anti-P-Thr172-AMPK (Cell Signaling Technologies, Catalogue No. 2535), anti-total Raptor (Cell Signaling Technologies, Catalogue No. 2280), anti-P-Ser792-Raptor (Cell Signaling Technologies, Catalogue No. 2083), anti-P-Thr56-eukaryotic elongation factor-2 (eEF2) (Cell Signaling Technologies, Catalogue No. 2331) and anti-total eEF2 (Cell Signaling Technologies, Catalogue No. 2332) antibodies were from the sources cited. Anti-total AMPKα1 and AMPKα2 antibodies were kindly provided by Grahame Hardie (University of Dundee, U.K.; see https://mrcppureagents.dundee.ac.uk/reagents-antibodies for details) or obtained from Bethyl Laboratories (Catalogue No. A300-507A for the anti-AMPKα1 antibody and Catalogue No. A300-508A for the anti-AMPKα2 antibody). For immunoblotting, the anti-total AMPKα antibody from Cell Signaling Technologies (Catalogue No. 2532) was used. Recombinant bacterially expressed AMPK (α1β1γ1) was activated with recombinant bacterially expressed LKB1 complex [47]. A mouse GPD2 cDNA clone provided in a pCMV6 vector was obtained from OriGene Technologies (Catalogue No. MC206608) and subcloned into a pGEX6p1 vector generously donated by Christopher Proud (South Australian Health & Medical Research Institute, University of Adelaide, Australia) for bacterial expression and purification of a Nt-GST fusion protein as previously described [48]. IHH cells were kindly provided by Bart Staels (Pasteur Institute & University of Lille, France). pcDNA3.1-Peredox-mCherry [49] was obtained from the Addgene collection (plasmid #32383) and Peredox-mCherry was subcloned using a Gateway strategy, into pTM978 (*PGK* > Gateway-IRES-Neo), a derivative of pTM898 [50] where the cloning site was replaced by a Gateway cassette, for production of lentiviral particles in HEK293T cells following a protocol similar to [51]. AMARA peptide was kindly synthesized by Dr. V. Stroobant (Ludwig Institute, Brussels).

Animals

All animal experiments were approved by the Université catholique de Louvain Brussels local ethics committee (reference numbers 2017/UCL/MD/016 and 2021/UCL/MD/028) and conducted in accordance with EU Directive 2010/63/EU for animal experiments. Adult C57BL/6J wild-type and AMPKβ1$^{-/-}$ male and female mice (4–6 months old) and adult male Wistar rats (12–15 weeks old) were obtained from the local animal facility. The animals were maintained on a 12 h light/12 h dark cycle with free access to food and water. Animals were fed a standard chow diet except for those used in Figure 5B, which were maintained on a 60%-fat HFD (D12492, Research Diets, U.S.A.) for 8 weeks before the experiment to induce insulin resistance. Animals were starved overnight before preparing hepatocytes for glucose production experiments or for isolation of liver mitochondria or for measurements of fasting glycemia. AMPKβ1$^{-/-}$ C57BL/6J mice were generated as previously described [52] and breeding pairs were kindly provided by Professor Bruce Kemp (St. Vincent's Institute, Melbourne, Australia) to start a colony in the local animal facility. Mice were anesthetized by intraperitoneal injection of 20 mg/kg Rompun (xylazine) + 100 mg/kg Imalgene (ketamine). Rats were anesthetized by intraperitoneal injection of 20 mg/kg Rompun (xylazine) + 20 mg/kg Dolethal (sodium pentobarbital).

Biochemical Journal (2022) 479 1317–1336
https://doi.org/10.1042/BCJ20220170

Mouse hepatocyte isolation and incubation

Mice were anesthetized and livers were washed with 50 ml of Krebs-HEPES pH 7.65 supplemented with 0.5 mM EDTA and digested with a solution of 50 ml of Krebs-HEPES, pH 7.65, containing 30 mg of collagenase from *Clostridium hystolyticum* (Sigma, Catalogue No. C5138) and 0.5 mM $CaCl_2$ by perfusion through the inferior vena cava at a rate of 5 ml/min as described [18]. Freshly isolated hepatocytes were incubated in Krebs-Ringer bicarbonate buffer (144 mM NaCl, 5.8 mM KCl, 1.4 mM $MgSO_4$, 1.4 mM KH_2PO_4, 25 mM $NaHCO_3$, 0.4 mM $CaCl_2$) that had been gassed with 95% O_2/5% CO_2 and supplemented with either 0.5 mM sodium octanoate or 10 mM glucose with or without compounds and substrates for glucose production as stated in the Figure legends. Typically, cells were distributed in 0.5 ml suspensions containing ~10^6 cells. After 30 min, the hepatocyte incubations were rapidly centrifuged to snap-freeze supernatants for glucose determination and pellets for protein or metabolite extraction using liquid N_2.

Glucose production

Typically, medium glucose from incubations conducted without exogenous glucose was measured spectrophotometrically [18] on a 0.3 ml aliquot of cell-free supernatant. Alternatively, for incubations in the presence of medium glucose, conversion of [U-^{14}C] lactate (specific activity 40 μCi/mmol) to [^{14}C] glucose was measured on a 0.2 ml aliquot of supernatant after anion removal on 1 ml Dowex 1X8 chloride columns washed with 1 ml methanol, followed by liquid scintillation counting [53]. For glucose production measurements when galactose or fructose were used as substrates, a glucose oxidase assay kit was used (Sigma Catalogue No. GAGO20).

Metabolite quantification by GC–MS

After incubation with the compounds and substrates as indicated in the figure legends, hepatocytes were collected by short centrifugation and rapidly washed with ice-cold 0.9% (w/v) NaCl before lysis in 1 ml of cold (−80°C) 50% (v/v) methanol kept on dry ice. Cold (−80°C) chloroform kept on dry ice (1 ml) was added and the samples were maintained on dry ice for 30 min. After centrifugation (20 000*g* × 10 min at 4°C) the polar upper phase was collected and vacuum-dried. Samples were derivatized with 20 μl of 2% (w/v pyridine) methoxyamine for 90 min at 30°C and with 40 μl of *N*-methyl-*N*-(trimethylsilyl) trifluoroacetamide (MSTFA) for 30 min at 37°C. Samples (1 μl) were injected in splitless mode for GC–MS with settings as described [54].

Cell lysis and immunoblotting

Following hepatocyte incubation, frozen cell pellets were lysed in 0.3 ml of buffer containing 50 mM HEPES pH 7.5, 1 mM EDTA, 1 mM EGTA, 0.1% (v/v) 2-mercaptoethanol, 10 mM NaF, 1 mM $Na_4P_2O_7$, 1 mM sodium β-glycerophosphate, 0.5 mM Na_3VO_3, 1 mM dithiothreitol, 0.1% (w/v) Triton X-100 and Complete^{TM} protease inhibitor cocktail (Roche). Extracts were centrifuged (20 000***g*** × 5 min at 4°C) and protein concentrations were measured by Bradford assay. For immunoblotting, 20 μg of protein samples were loaded on 7.5% (w/v) polyacrylamide gels. Following SDS–PAGE, proteins were transferred to PVDF membranes, which were then blocked in Tris-buffered saline (TBS) containing 0.1% (v/v) Tween and 5% (w/v) bovine serum albumin (BSA). The membranes were incubated overnight at 4°C with the indicated primary antibodies diluted in blocking buffer, then washed extensively before and after incubation for 1 h with horseradish peroxidase-conjugated secondary antibodies. Anti-total ACC, anti-phospho ACC, anti-total Raptor, anti-phospho Raptor, anti-total AMPKβ1 and anti-phospho AMPK were used at a dilution of 1 : 1000. Anti-total eEF2 was used at a dilution of 1 : 5000. Anti-GAPDH and anti-phospho eEF2 were used at a dilution of 1 : 20 000. Anti-total AMPKα1 + AMPKα2 antibodies were used at a dilution of 1 : 10 000. Immunodetection was by ECL Classico substrate (Merck Millipore). Immunoblots were quantified by densitometry using ImageJ software.

Isolation of rat liver mitochondria for measurements of OCR and mitochondrial pyruvate uptake

Mitochondria were isolated from the liver of an overnight starved rat in mitochondrial assay solution (MAS) containing 2 mM Hepes, pH 7.2, 70 mM sucrose, 220 mM mannitol, 10 mM KH_2PO_4, 5 mM $MgCl_2$, 1 mM EGTA. After Dounce homogenization in 40 ml of MAS and centrifugation (600***g*** × 10 min, 4°C), mitochondria were pelleted from the supernatant (10 000***g*** × 10 min, 4°C) and washed twice. Mitochondria were resuspended for protein estimation and diluted in MAS with 0.2% (w/v) BSA to load 4 μg per well in a Seahorse^{TM} 96 well

Biochemical Journal (2022) 479 1317–1336
https://doi.org/10.1042/BCJ20220170

culture plate. After centrifugation (2000*g* × 20 min, 4°C), mitochondria were pre-incubated for 60 min at 37°C in a CO_2-free incubator in the presence of the different compounds as indicated in the figure legends. Standard substrates for complex I-dependent baseline measurements (2 mM ADP, 2.5 mM malate and 10 mM pyruvate) were added just before the start of the experiment. To determine GPD2-dependent OCR, 10 mM Gro3P was used as substrate and 100 μM TMPD together with 10 mM ascorbate was used as electron donor to determine complex IV-dependent OCR. At least three cycles of mixing/measuring (3 min/4 min) were performed for each injection and complex-dependent respiration was calculated by the difference between the mean OCR before versus after injections. Mitochondrial uptake of 0.2 mM [^{14}C] pyruvate was measured for 2 min at 4°C after 10 min pre-incubation in respiration buffer (3 mM Hepes pH 7.4, 120 mM KCl, 5 mM KH_2PO_4, 1 mM EGTA, 0.1 mM malate, 1 μM antimycin, 1 μM rotenone and 3 mM ascorbate + 3 μM TMPD) to create an artificial proton gradient required for pyruvate transport by the MPC using an inhibitor-stop technique [55].

Enzyme assays

AMPKα1 + AMPKα2 activity immunoprecipitated from 100 μg of hepatocyte lysates was measured as described [15] in kinase assay buffer (10 mM MOPS pH 7.0, 0.5 mM EDTA, 10 mM magnesium acetate, 5 mM dithiothreitol, 0.2 mM AMP) by measuring ^{32}P incorporation from 0.1 mM [γ-^{32}P] ATP (specific radioactivity 1000 cpm/pmol) into 200 μM substrate 'AMARA' peptide (sequence AMARAASAAALRRR) [15]. Cell lysates were assayed for PKA in the same buffer, by measuring phosphorylation of a heart PFK-2-derived substrate peptide (sequence PVRMRRNSFT) with or without PKA inhibitor peptide (sequence TYADFIASGRTGRRNAIHD) present, as described [15]. Purified recombinant GPD2 was assayed spectrophotometrically by decoloration of the blue dye 2,6-Dichlorophenolindophenol (DCPIP) used as artificial electron acceptor [56]. After adding 5–10 μg GST-mGPD2 per 1 ml of 50 mM Tris–HCl pH 7.4 containing 50 mM KCl, 1 mM EDTA, 1 mM Gro3P, 10 mM DCPIP absorbance was followed at 600 nm over 10 min at room temperature. Alternatively, GPD2 activity in rat liver mitochondria (~1 mg of total protein) was measured by reduction of cytochrome c (10 mg/ml) added to 0.9 ml of 50 mM potassium phosphate buffer pH 7.6 containing 250 mM sucrose, 1 mM EDTA, 25 μM sodium azide, 1 mM KCN, 0.2% (w/v) BSA, 5 mM Gro3P and following absorbance at 550 nm. Rabbit muscle GPD1 (Sigma–Aldrich, Catalogue N° 10127752001) activity was measured by following NADH oxidation in 1 ml of 50 mM Tris–HCl buffer pH 7.4 containing 1 mM EDTA, 1 mM dihydroxyacetone phosphate and 0.2 mM NADH spectrophotometrically at 340 nm. Pig heart MDH2 (Sigma–Aldrich, Catalogue N°10127256001) and plant MDH1 [57] were assayed by following NADH oxidation in 1 ml of 0.1 M potassium phosphate buffer pH 7.4 containing 5 mM $MgCl_2$, 1 mM oxaloacetate and 0.2 mM NADH spectrophotometrically at 340 nm. Rabbit muscle LDH (Sigma–Aldrich, Catalogue N° 26230325) was assayed by following NADH oxidation in 1 ml of 50 mM Tris–HCl buffer pH 7.4 containing 0.2 M NaCl, 0.2 mM NADH and 1 mM pyruvate spectrophotometrically at 340 nm.

Live-cell monitoring of cytosolic NADH : NAD$^+$ ratio

IHH cells were lentivirally transduced with the NADH-sensitive Peredox probe under the control of a phosphoglycerate kinase (*PGK*) promoter. Selection for neomycin/G418 resistance was maintained until all cells were positive for stable red fluorescence due to the mCherry moiety of the probe. For real-time monitoring of NADH-sensitive green fluorescence (microscope: Zeiss Axiovert 200 M, software: Zeiss Axiovision 4.8, filters: FITC channel with excitation at 480 nm/emission at 535 nm, objective: Zeiss Fluar 20×, camera: Zeiss AxioCam MRm) based on [42], cells were plated on 15 mm-diameter circular glass cover slips and transferred to Krebs-Ringer buffer supplemented with 5 mM Hepes, pH 7.4 and 10 mM glucose for 15 min prior to analysis. At least 30 cells were selected for parallel measurement of instant fluorescence over initial fluorescence (F/F_0) ratios. After the establishment of a stable baseline, data were acquired every 5 s for at least 5 min after addition of compounds or substrates and then every 10–20 s for up to 30 min. For long-term incubations up to 24 h, IHH cells were cultured in standard DMEM media in transparent 96 well-plates (eight wells per condition) and the Incucyte© in-incubator imaging system (Sartorius) was used to acquire phase-contrast and fluorescent (green for analysis at 405/525 nm and red for normalization at 580/630 nm) pictures every hour and relative intensity was calculated as instant fluorescence over initial fluorescence (F/F_0) ratios.

In vitro phosphorylation

Recombinant GST-GPD2 (5 μg) was incubated for 1 h with 1U of activated recombinant AMPK in 50 μl of kinase assay buffer (see AMPK assay). For measurements of the stoichiometry of phosphorylation, proteins

were separated by SDS–PAGE in 7.5% (w/v) polyacrylamide gels. Gels were stained using PageBlue (Thermo Fisher Scientific) for protein band quantification by Odyssey (Licor) infrared imaging. Bands were then excised from the gels for measurement of ^{32}P-incorporation or for phosphorylation site identification as described previously [58]. Briefly, tryptic peptides were separated by reverse-phase HPLC and radioactive peaks were analyzed by LC–MS/MS. Multi-stage activation was enabled for phosphate neutral loss of 98, 49 or 32.66 with respect to the precursor m/z. Peak lists were generated and searched using SequestHT and PhosphoRS 3.1 against a home-made protein database containing the mouse GPD2 sequence from Uniprot. Phosphorylation site identification was performed as described [58] and validated manually.

Virtual docking experiments

A structural model of *Mus musculus* GPD2 was generated using the I-TASSER server for structure prediction [59], with the 2.3 Å crystal structure of *Streptococcus sp.* α-glycerophosphate oxidase (PDB ID: 2RGH) as template model [40] and local structure quality of the model further improved in the GalaxyRefine web server [60]. Compound 991 for *in silico* docking was prepared in JLigand [61] and restraints and hydrogens generated using ProDrg [62] and AceDrg [63]. A basic docking approach in Autodock Vina [64] was used for simulated docking experiments, with the entire protein molecule enclosed within the docking search area.

In vivo monitoring of glycemia and IPPTT

Mice were starved overnight and glucose concentrations were measured on blood drops taken from the tip of the tail at the indicated time intervals using a hand-held strip-glucometer (Freestyle Lite, Abbott, Belgium). For compound treatment, 2 h before starting measurements, 991 (10 mg per kg of bodyweight) or DMSO vehicle control were injected intraperitoneally after dissolving in ∼400 µl/mouse of saline (0.9% w/v NaCl) with 10 mM NaOH to improve compound solubility as described [65]. For IPPTT, sodium pyruvate was dissolved in water at neutral pH and injected intraperitoneally (∼500 µl per mouse) at a dose of 1 g per kg of bodyweight.

Statistical analysis

The results are expressed as means ± S.E.M. of the number of independent experiments/technical replicates indicated in the figure legends. All two-group comparisons were done by paired two-sided Student's *t*-tests and multi-group comparisons were carried out by ANOVA followed by appropriate post-hoc tests, and $P < 0.05$ was considered significant. GraphPad Prism software was used for statistical analysis and generation of graphics.

Data Availability

All relevant data are contained within the main article and its Supplementary Files.

Competing Interests

G.R.S. has received research funding from Esperion Therapeutics, Espervita Therapeutics, Poxel Pharmaceuticals and Novo Nordisk, honoraria and/or consulting fees from Astra Zeneca, Eli-Lilly, Esperion Therapeutics, Poxel Pharmaceuticals, Merck and is a founder and shareholder of Espervita Therapeutics.

Funding

The work was funded by the Fund for Medical Scientific Research (FNRS, Belgium) grant numbers T.0008.15 and T.0208.20. G.R.S. is supported by a Canada Research Chair and the J Bruce Duncan Endowed Chair in Metabolic Diseases and program grants from the Canadian Institutes of Health Research (201709FDN-CEBA-116200) and Diabetes Canada (DI-5-17-5302-GS).

CRediT Author Contribution

Mark H. Rider: Conceptualization, Supervision, Funding acquisition, Writing — review and editing. **Manuel Johanns:** Conceptualization, Data curation, Investigation, Writing — original draft. **Cyril Corbet:** Supervision, Investigation. **Roxane Jacobs:** Investigation. **Melissa Drappier:** Resources, Supervision, Methodology. **Guido T. Bommer:** Resources, Supervision, Methodology. **Gaëtan Herinckx:** Investigation, Methodology. **Didier Vertommen:** Formal analysis, Supervision, Methodology. **Nicolas Tajeddine:** Supervision, Methodology. **David Young:** Formal analysis, Investigation. **Joris Messens:** Supervision. **Olivier Feron:** Supervision, Methodology.

Biochemical Journal (2022) **479** 1317–1336
https://doi.org/10.1042/BCJ20220170

Gregory R. Steinberg: Resources, Writing — review and editing. **Louis Hue:** Conceptualization, Supervision, Writing — original draft.

Acknowledgements

We thank Professor Bruce E. Kemp (St. Vincent's Institute, Melbourne, Australia) for providing breeding pairs of AMPKβ1$^{-/-}$ mice.

Abbreviations

ACC, acetyl-CoA carboxylase; AICAR, 5-aminoimidazole-4-carboxamide riboside; AMPK, AMP-activated protein kinase; cAMP, adenosine 3′,5′-cyclic monophosphate; FBPase-1, fructose-1,6-bisphosphatase; G6Pase, glucose-6-phosphatase; GNG, gluconeogenesis; GPD1/2, *sn*-glycerol-3-phosphate dehydrogenase-1/2; HFD, high-fat diet; HGP, hepatic glucose production; IHH, immortalized human hepatocyte; IPPTT, intraperitoneal pyruvate tolerance test; LDH, lactate dehydrogenase; LKB1, liver kinase B1; MDH1/2, malate dehydrogenase-1/2; MPC, mitochondrial pyruvate carrier; PDE4B, cyclic nucleotide phosphodiesterase-4B; PEPCK, phosphoenolpyruvate carboxykinase; PKA, cAMP-dependent protein kinase; T2D, type 2 diabetes.

References

1 DeFronzo, R.A. and Tripathy, D. (2009) Skeletal muscle insulin resistance is the primary defect in type 2 diabetes. *Diabetes Care* **32**, S157–S163 https://doi.org/10.2337/dc09-S302
2 Roden, M. and Shulman, G.I. (2019) The integrative biology of type 2 diabetes. *Nature* **576**, 51–60 https://doi.org/10.1038/s41586-019-1797-8
3 Girard, J. (2017) Glucagon, a key factor in the pathophysiology of type 2 diabetes. *Biochimie* **143**, 33–36 https://doi.org/10.1016/j.biochi.2017.10.004
4 Cahill, Jr, G.F. (2006) Fuel metabolism in starvation. *Annu. Rev. Nutr.* **26**, 1–22 https://doi.org/10.1146/annurev.nutr.26.061505.111258
5 Authier, F. and Desbuquois, B. (2008) Glucagon receptors. *Cell. Mol. Life Sci.* **65**, 1880–1899 https://doi.org/10.1007/s00018-008-7479-6
6 Exton, J.H. (1987) Mechanisms of hormonal regulation of hepatic glucose metabolism. *Diabetes Metab. Rev.* **3**, 163–183 https://doi.org/10.1002/dmr.5610030108
7 Hers, H.G. and Van Schaftingen, E. (1984) Protein phosphorylation in the control of glycolysis and gluconeogenesis in the liver. *Adv. Cyclic Nucleotide Protein Phosphorylation Res.* **17**, 343–349 PMID:6328924
8 Pilkis, S.J., el-Maghrabi, M.R. and Claus, T.H. (1988) Hormonal regulation of hepatic gluconeogenesis and glycolysis. *Annu. Rev. Biochem.* **57**, 755–783 https://doi.org/10.1146/annurev.bi.57.070188.003543
9 Sakakibara, R., Kitajima, S. and Uyeda, K. (1984) Differences in kinetic properties of phospho and dephospho forms of fructose-6-phosphate, 2-kinase and fructose 2,6-bisphosphatase. *J. Biol. Chem.* **259**, 41–46 https://doi.org/10.1016/S0021-9258(17)43618-0
10 El-Maghrabi, M.R., Haston, W.S., Flockhart, D.A., Claus, T.H. and Pilkis, S.J. (1980) Studies on the phosphorylation and dephosphorylation of L-type pyruvate kinase by the catalytic subunit of cyclic AMP-dependent protein kinase. *J. Biol. Chem.* **255**, 668–675 https://doi.org/10.1016/S0021-9258(19)86229-4
11 Feliú, J.E., Hue, L. and Hers, H.G. (1976) Hormonal control of pyruvate kinase activity and of gluconeogenesis in isolated hepatocytes. *Proc. Natl Acad. Sci. U.S.A.* **73**, 2762–2766 https://doi.org/10.1073/pnas.73.8.2762
12 Argaud, D., Zhang, Q., Pan, W., Maitra, S., Pilkis, S.J. and Lange, A.J. (1996) Regulation of rat liver glucose-6-phosphatase gene expression in different nutritional and hormonal states: gene structure and 5′-flanking sequence. *Diabetes* **45**, 1563–1571 https://doi.org/10.2337/diab.45.11.1563
13 Hanson, R.W. and Reshef, L. (1997) Regulation of phosphoenolpyruvate carboxykinase (GTP) gene expression. *Annu. Rev. Biochem.* **66**, 581–611 https://doi.org/10.1146/annurev.biochem.66.1.581
14 Hardie, D.G. (2017) Targeting an energy sensor to treat diabetes. *Science* **357**, 455–456 https://doi.org/10.1126/science.aao1913
15 Johanns, M., Lai, Y.C., Hsu, M.F., Jacobs, R., Vertommen, D., Van Sande, J. et al. (2016) AMPK antagonizes hepatic glucagon-stimulated cyclic AMP signalling via phosphorylation-induced activation of cyclic nucleotide phosphodiesterase 4B. *Nat. Commun.* **7**, 10856 https://doi.org/10.1038/ncomms10856
16 Winder, W.W. and Hardie, D.G. (1999) AMP-activated protein kinase, a metabolic master switch: possible roles in type 2 diabetes. *Am. J. Physiol.* **277**, E1–E10 https://doi.org/10.1152/ajpendo.1999.277.1.E1
17 Zhou, G., Myers, R., Li, Y., Chen, Y., Shen, X., Fenyk-Melody, J. et al. (2001) Role of AMP-activated protein kinase in mechanism of metformin action. *J. Clin. Invest.* **108**, 1167–1174 https://doi.org/10.1172/JCI13505
18 Foretz, M., Hebrard, S., Leclerc, J., Zarrinpashneh, E., Soty, M., Mithieux, G. et al. (2010) Metformin inhibits hepatic gluconeogenesis in mice independently of the LKB1/AMPK pathway via a decrease in hepatic energy state. *J. Clin. Invest.* **120**, 2355–2369 https://doi.org/10.1172/JCI40671
19 Guigas, B., Bertrand, L., Taleux, N., Foretz, M., Wiernsperger, N., Vertommen, D. et al. (2006) 5-Aminoimidazole-4-carboxamide-1-beta-D-ribofuranoside and metformin inhibit hepatic glucose phosphorylation by an AMP-activated protein kinase-independent effect on glucokinase translocation. *Diabetes* **55**, 865–874 https://doi.org/10.2337/diabetes.55.04.06.db05-1178
20 Andreelli, F., Foretz, M., Knauf, C., Cani, P.D., Perrin, C., Iglesias, M.A. et al. (2006) Liver adenosine monophosphate-activated kinase-alpha2 catalytic subunit is a key target for the control of hepatic glucose production by adiponectin and leptin but not insulin. *Endocrinology* **147**, 2432–2441 https://doi.org/10.1210/en.2005-0898
21 Foretz, M., Ancellin, N., Andreelli, F., Saintillan, Y., Grondin, P., Kahn, A. et al. (2005) Short-term overexpression of a constitutively active form of AMP-activated protein kinase in the liver leads to mild hypoglycemia and fatty liver. *Diabetes* **54**, 1331–1339 https://doi.org/10.2337/diabetes.54.5.1331
22 Shaw, R.J., Lamia, K.A., Vasquez, D., Koo, S.H., Bardeesy, N., Depinho, R.A. et al. (2005) The kinase LKB1 mediates glucose homeostasis in liver and therapeutic effects of metformin. *Science* **310**, 1642–1646 https://doi.org/10.1126/science.1120781

23 Foretz, M., Guigas, B. and Viollet, B. (2019) Understanding the glucoregulatory mechanisms of metformin in type 2 diabetes mellitus. *Nat. Rev. Endocrinol.* **15**, 569–589 https://doi.org/10.1038/s41574-019-0242-2
24 Corton, J.M., Gillespie, J.G., Hawley, S.A. and Hardie, D.G. (1995) 5-aminoimidazole-4-carboxamide ribonucleoside. A specific method for activating AMP-activated protein kinase in intact cells? *Eur. J. Biochem.* **229**, 558–565 https://doi.org/10.1111/j.1432-1033.1995.tb20498.x
25 Langendorf, C.G. and Kemp, B.E. (2015) Choreography of AMPK activation. *Cell Res.* **25**, 5–6 https://doi.org/10.1038/cr.2014.163
26 Cool, B., Zinker, B., Chiou, W., Kifle, L., Cao, N., Perham, M. et al. (2006) Identification and characterization of a small molecule AMPK activator that treats key components of type 2 diabetes and the metabolic syndrome. *Cell Metab.* **3**, 403–416 https://doi.org/10.1016/j.cmet.2006.05.005
27 Sanders, M.J., Ali, Z.S., Hegarty, B.D., Heath, R., Snowden, M.A. and Carling, D. (2007) Defining the mechanism of activation of AMP-activated protein kinase by the small molecule A-769662, a member of the thienopyridone family. *J. Biol. Chem.* **282**, 32539–32548 https://doi.org/10.1074/jbc.M706543200
28 Xiao, B., Sanders, M.J., Carmena, D., Bright, N.J., Haire, L.F., Underwood, E. et al. (2013) Structural basis of AMPK regulation by small molecule activators. *Nat. Commun.* **4**, 3017 https://doi.org/10.1038/ncomms4017
29 Lai, Y.C., Kviklyte, S., Vertommen, D., Lantier, L., Foretz, M., Viollet, B. et al. (2014) A small-molecule benzimidazole derivative that potently activates AMPK to increase glucose transport in skeletal muscle: comparison with effects of contraction and other AMPK activators. *Biochem. J.* **460**, 363–375 https://doi.org/10.1042/BJ20131673
30 Ngoei, K.R.W., Langendorf, C.G., Ling, N.X.Y., Hoque, A., Varghese, S., Camerino, M.A. et al. (2018) Structural determinants for small-Molecule activation of skeletal muscle AMPK alpha2beta2gamma1 by the glucose importagog SC4. *Cell Chem. Biol.* **25**, 728–737.e729 https://doi.org/10.1016/j.chembiol.2018.03.008
31 Myers, R.W., Guan, H.P., Ehrhart, J., Petrov, A., Prahalada, S., Tozzo, E. et al. (2017) Systemic pan-AMPK activator MK-8722 improves glucose homeostasis but induces cardiac hypertrophy. *Science* **357**, 507–511 https://doi.org/10.1126/science.aah5582
32 Cokorinos, E.C., Delmore, J., Reyes, A.R., Albuquerque, B., Kjobsted, R., Jorgensen, N.O. et al. (2017) Activation of skeletal muscle AMPK promotes glucose disposal and glucose lowering in Non-human primates and mice. *Cell Metab.* **25**, 1147–1159.e1110 https://doi.org/10.1016/j.cmet.2017.04.010
33 Steneberg, P., Lindahl, E., Dahl, U., Lidh, E., Straseviciene, J., Backlund, F. et al. (2018) PAN-AMPK activator O304 improves glucose homeostasis and microvascular perfusion in mice and type 2 diabetes patients. *JCI Insight* **3**, e99114 https://doi.org/10.1172/jci.insight.99114
34 Madiraju, A.K., Qiu, Y., Perry, R.J., Rahimi, Y., Zhang, X.M., Zhang, D. et al. (2018) Metformin inhibits gluconeogenesis via a redox-dependent mechanism *in vivo*. *Nat. Med.* **24**, 1384–1394 https://doi.org/10.1038/s41591-018-0125-4
35 Baba, H., Zhang, X.J. and Wolfe, R.R. (1995) Glycerol gluconeogenesis in fasting humans. *Nutrition* **11**, 149–153 https://pubmed.ncbi.nlm.nih.gov/7647479/
36 Terrettaz, J. and Jeanrenaud, B. (1990) Contribution of glycerol and alanine to basal hepatic glucose production in the genetically obese (fa/fa) rat. *Biochem. J.* **270**, 803–807 https://doi.org/10.1042/bj2700803
37 Hunter, R.W., Hughey, C.C., Lantier, L., Sundelin, E.I., Peggie, M., Zeqiraj, E. et al. (2018) Metformin reduces liver glucose production by inhibition of fructose-1-6-bisphosphatase. *Nat. Med.* **24**, 1395–1406 https://doi.org/10.1038/s41591-018-0159-7
38 Madiraju, A.K., Erion, D.M., Rahimi, Y., Zhang, X.M., Braddock, D.T., Albright, R.A. et al. (2014) Metformin suppresses gluconeogenesis by inhibiting mitochondrial glycerophosphate dehydrogenase. *Nature* **510**, 542–546 https://doi.org/10.1038/nature13270
39 Mráček, T., Drahota, Z. and Houštěk, J. (2013) The function and the role of the mitochondrial glycerol-3-phosphate dehydrogenase in mammalian tissues. *Biochim. Biophys. Acta* **1827**, 401–410 https://doi.org/10.1016/j.bbabio.2012.11.014
40 Colussi, T., Parsonage, D., Boles, W., Matsuoka, T., Mallett, T.C., Karplus, P.A. et al. (2008) Structure of alpha-glycerophosphate oxidase from Streptococcus sp.: a template for the mitochondrial alpha-glycerophosphate dehydrogenase. *Biochemistry* **47**, 965–977 https://doi.org/10.1021/bi701685u
41 Lee, Y.J., Jeschke, G.R., Roelants, F.M., Thorner, J. and Turk, B.E. (2012) Reciprocal phosphorylation of yeast glycerol-3-phosphate dehydrogenases in adaptation to distinct types of stress. *Mol. Cell. Biol.* **32**, 4705–4717 https://doi.org/10.1128/MCB.00897-12
42 Masia, R., McCarty, W.J., Lahmann, C., Luther, J., Chung, R.T., Yarmush, M.L. et al. (2018) Live cell imaging of cytosolic NADH/NAD(+) ratio in hepatocytes and liver slices. *Am. J. Physiol. Gastrointest. Liver Physiol.* **314**, G97–g108 https://doi.org/10.1152/ajpgi.00093.2017
43 Samanez, C.H., Caron, S., Briand, O., Dehondt, H., Duplan, I., Kuipers, F. et al. (2012) The human hepatocyte cell lines IHH and HepaRG: models to study glucose, lipid and lipoprotein metabolism. *Arch. Physiol. Biochem.* **118**, 102–111 https://doi.org/10.3109/13813455.2012.683442
44 Wu, J., Puppala, D., Feng, X., Monetti, M., Lapworth, A.L. and Geoghegan, K.F. (2013) Chemoproteomic analysis of intertissue and interspecies isoform diversity of AMP-activated protein kinase (AMPK). *J. Biol. Chem.* **288**, 35904–35912 https://doi.org/10.1074/jbc.M113.508747
45 Halestrap, A.P. and Denton, R.M. (1974) Specific inhibition of pyruvate transport in rat liver mitochondria and human erythrocytes by alpha-cyano-4-hydroxycinnamate. *Biochem. J.* **138**, 313–316 https://doi.org/10.1042/bj1380313
46 Li, Y.Y., Yu, L.F., Zhang, L.N., Qiu, B.Y., Su, M.B., Wu, F. et al. (2013) Novel small-molecule AMPK activator orally exerts beneficial effects on diabetic db/db mice. *Toxicol. Appl. Pharmacol.* **273**, 325–334 https://doi.org/10.1016/j.taap.2013.09.006
47 Bultot, L., Guigas, B., Von Wilamowitz-Moellendorff, A., Maisin, L., Vertommen, D., Hussain, N. et al. (2012) AMP-activated protein kinase phosphorylates and inactivates liver glycogen synthase. *Biochem. J.* **443**, 193–203 https://doi.org/10.1042/BJ20112026
48 Johanns, M., Pyr Dit Ruys, S., Houddane, A., Vertommen, D., Herinckx, G., Hue, L. et al. (2017) Direct and indirect activation of eukaryotic elongation factor 2 kinase by AMP-activated protein kinase. *Cell Signal.* **36**, 212–221 https://doi.org/10.1016/j.cellsig.2017.05.010
49 Hung, Y.P., Albeck, J.G., Tantama, M. and Yellen, G. (2011) Imaging cytosolic NADH-NAD(+) redox state with a genetically encoded fluorescent biosensor. *Cell Metab.* **14**, 545–554 https://doi.org/10.1016/j.cmet.2011.08.012
50 Sorgeloos, F., Jha, B.K., Silverman, R.H. and Michiels, T. (2013) Evasion of antiviral innate immunity by Theiler's virus L* protein through direct inhibition of RNase L. *PLoS Pathog.* **9**, e1003474 https://doi.org/10.1371/journal.ppat.1003474
51 Kreit, M., Paul, S., Knoops, L., De Cock, A., Sorgeloos, F. and Michiels, T. (2014) Inefficient type I interferon-mediated antiviral protection of primary mouse neurons is associated with the lack of apolipoprotein l9 expression. *J. Virol.* **88**, 3874–3884 https://doi.org/10.1128/JVI.03018-13
52 Dzamko, N., van Denderen, B.J., Hevener, A.L., Jorgensen, S.B., Honeyman, J., Galic, S. et al. (2010) AMPK beta1 deletion reduces appetite, preventing obesity and hepatic insulin resistance. *J. Biol. Chem.* **285**, 115–122 https://doi.org/10.1074/jbc.M109.056762

Biochemical Journal (2022) **479** 1317–1336
https://doi.org/10.1042/BCJ20220170

53 Hue, L., Felíu, J.E. and Hers, H.G. (1978) Control of gluconeogenesis and of enzymes of glycogen metabolism in isolated rat hepatocytes. A parallel study of the effect of phenylephrine and of glucagon. *Biochem. J.* **176**, 791–797 https://doi.org/10.1042/bj1760791
54 Collard, F., Baldin, F., Gerin, I., Bolsée, J., Noël, G., Graff, J. et al. (2016) A conserved phosphatase destroys toxic glycolytic side products in mammals and yeast. *Nat. Chem. Biol.* **12**, 601–607 https://doi.org/10.1038/nchembio.2104
55 Halestrap, A.P. (1975) The mitochondrial pyruvate carrier. Kinetics and specificity for substrates and inhibitors. *Biochem. J.* **148**, 85–96 https://doi.org/10.1042/bj1480085
56 Gardner, R.S. (1974) A sensitive colorimetric assay for mitochondrial alpha-glycerophosphate dehydrogenase. *Anal. Biochem.* **59**, 272–276 https://doi.org/10.1016/0003-2697(74)90033-5
57 Huang, J., Niazi, A.K., Young, D., Rosado, L.A., Vertommen, D., Bodra, N. et al. (2018) Self-protection of cytosolic malate dehydrogenase against oxidative stress in arabidopsis. *J. Exp. Bot.* **69**, 3491–3505 https://doi.org/10.1093/jxb/erx396
58 Vertommen, D., Rider, M., Ni, Y., Waelkens, E., Merlevede, W., Vandenheede, J.R. et al. (2000) Regulation of protein kinase D by multisite phosphorylation. identification of phosphorylation sites by mass spectrometry and characterization by site-directed mutagenesis. *J. Biol. Chem.* **275**, 19567–19576 https://doi.org/10.1074/jbc.M001357200
59 Yang, J. and Zhang, Y. (2015) I-TASSER server: new development for protein structure and function predictions. *Nucleic Acids Res.* **43**, W174–W181 https://doi.org/10.1093/nar/gkv342
60 Heo, L., Park, H. and Seok, C. (2013) Galaxyrefine: protein structure refinement driven by side-chain repacking. *Nucleic Acids Res.* **41**, W384–W388 https://doi.org/10.1093/nar/gkt458
61 Lebedev, A.A., Young, P., Isupov, M.N., Moroz, O.V., Vagin, A.A. and Murshudov, G.N. (2012) JLigand: a graphical tool for the CCP4 template-restraint library. *Acta Crystallogr. D Biol. Crystallogr.* **68**, 431–440 https://doi.org/10.1107/S090744491200251X
62 Schüttelkopf, A.W. and van Aalten, D.M. (2004) PRODRG: a tool for high-throughput crystallography of protein-ligand complexes. *Acta Crystallogr. D Biol. Crystallogr.* **60**, 1355–1363 https://doi.org/10.1107/S0907444904011679
63 Long, F., Nicholls, R.A., Emsley, P., Graæulis, S., Merkys, A., Vaitkus, A. et al. (2017) AceDRG: a stereochemical description generator for ligands. *Acta Crystallogr. D Struct. Biol.* **73**, 112–122 https://doi.org/10.1107/S2059798317000067
64 Trott, O. and Olson, A.J. (2010) Autodock Vina: improving the speed and accuracy of docking with a new scoring function, efficient optimization, and multithreading. *J. Comput. Chem.* **31**, 455–461 https://doi.org/10.1002/jcc.21334
65 Choumessi, A.T., Johanns, M., Beaufay, C., Herent, M.F., Stroobant, V., Vertommen, D. et al. (2019) Two isoprenylated flavonoids from Dorstenia psilurus activate AMPK, stimulate glucose uptake, inhibit glucose production and lower glycemia. *Biochem. J.* **476**, 3687–3704 https://doi.org/10.1042/BCJ20190326